

Author response to referee comments for the manuscript titled “Multi-Satellite Retrieval of SSA using OMI-MODIS algorithm”

We thank the referee for the valuable comments and suggestions in improving this manuscript. Please note that author comments (AC) are in red font color. The modified manuscript along with the author marked changes are provided after the authors’ response.

Anonymous Referee #2

Abstract:

RC: Line 7: “... and can be a determinant factor in the estimation of aerosol radiative forcing”

AC: The statement has been modified accordingly.

RC: Line 22: “cruise-based measurements”

AC: The statement has been modified accordingly.

Introduction:

RC: Line 29: “certain aerosol types such as carbonaceous aerosols emitted from biomass burning”

AC: The statement has been modified accordingly.

RC: Line 86: “...and uncertainty in the assumption of spectral surface albedo”

AC: The statement has been modified accordingly.

RC: Line 91: Levy et al. (2013) should be referenced here.

AC: The reference has been added.

RC: Line 93-94: The statement "This removes any a priori assumption made by the OMI algorithm regarding aerosol model" is incorrect. Use of MODIS AOD as an input make the UV algorithm free to retrieve ALH along with SSA. The aerosol type, particle size distribution, refractive indices, and surface albedo still need to be assumed, as in the standard OMI algorithm.

AC: The statement has been modified accordingly.

Summary and Conclusion:

RC: Line 485: “...aerosol properties such as aerosol optical depth..”

AC: The statement has been modified accordingly.

RC: Line 486-487: "...aerosol composition, size, and the wavelength..."

AC: The statement has been modified accordingly.

RC: Line 490: "However, these retrievals might be affected by the cloud contamination due to the coarser pixel resolution of 13 x 24 km-square...and are sensitive to the assumption of aerosol layer height in the inversion procedure"

AC: The statement has been modified accordingly.

RC: Line 495: "...much larger spatial and temporal scales"

AC: The statement has been modified accordingly.

RC: Line 497-499: "...large amounts of aerosols with moderate to high absorption capacity"

AC: The statement has been modified accordingly.

RC: Line 501: "...over ATL for more than 80% of the time"

AC: The statement has been modified accordingly.

RC: Line 503: Discrepancy in SSA over the Arabian Sea could also be partly attributed to the sub-pixel cloud contamination during summer-monsoon season.

AC: The statement has been added accordingly.

RC: Line 513: "...due to the presence of elevated aerosols not sampled by surface instrument"

AC: The statement has been modified accordingly.

1 Multi-Satellite Retrieval of SSA using OMI-MODIS algorithm

2 Kruthika Eswaran^{1,2*}, Sreedharan Krishnakumari Satheesh^{1,2} and Jayaraman Srinivasan^{1,2}

3 ¹ Centre for Atmospheric and Oceanic Sciences, Indian Institute of Science, Bangalore, India

4 ² Divecha Centre for Climate Change, Indian Institute of Science, Bangalore, India

5 *Correspondence to: Kruthika Eswaran (kruthika.eswaran89@gmail.com)

6 **Abstract** - Single scattering albedo (SSA) represents a unique identification of aerosol type and
7 [can be a determinant factor in the estimation of](#) aerosol radiative forcing. However, SSA
8 retrievals are highly uncertain due to cloud contamination and aerosol composition. The recent
9 improvement in the SSA retrieval algorithm has combined the superior cloud-masking technique
10 of the Moderate Resolution Imaging Spectroradiometer (MODIS) and the better sensitivity of the
11 Ozone Monitoring Instrument (OMI) to aerosol absorption. The combined OMI-MODIS
12 algorithm has been validated over a small spatial and temporal scale only. The present study
13 validates the algorithm over global oceans for the period 2008-2012. The geographical
14 heterogeneity in the aerosol type and concentration over the Atlantic Ocean, the Arabian Sea and
15 the Bay of Bengal was useful to delineate the effect of aerosol type on the retrieval algorithm.
16 We also noted that OMI overestimated SSA when absorbing aerosols were present closer to the
17 surface. We attribute this overestimation to data discontinuity in the aerosol height climatology
18 derived from Cloud-Aerosol Lidar and Infrared Pathfinder Satellite Observations (CALIPSO)
19 satellite. OMI uses pre-defined aerosol heights over regions where CALIPSO climatology is not
20 present leading to overestimation of SSA. The importance of aerosol height was also studied
21 using the Santa Barbara DISORT radiative transfer (SBDART) model. The results from the joint
22 retrieval were validated with [groundcruise](#)-based measurements ~~and~~ [.i](#) It was seen that OMI-
23 MODIS SSA retrievals performed better than OMI only retrieval over the Bay of Bengal during

24 winter when the aerosols are present closer to the surface. Discrepancy between satellite
25 retrievals and cruise measurements was seen when elevated aerosols are present which might not
26 be detected by the cruise instruments.

27 **1. Introduction**

28 Aerosols of different types are spatially distributed heterogeneously and at different altitudes in
29 the atmosphere. Depending upon their properties, certain aerosols types such as carbonaceous
30 aerosols emitted from biomass burning (~~biomass and carbon~~) warm the atmosphere by absorbing
31 radiation, while other aerosols (~~sea salts and sulphates~~) types such as sea salt emitted from the
32 oceans cool the atmosphere by scattering radiation (Ramanathan et al., 2001). Due to the
33 opposing effects on the atmosphere aerosols can have either net warming or cooling effect on the
34 global climate depending upon the aerosol type, concentration and vertical distribution. Effect of
35 natural and anthropogenic aerosols on the global climate is measured by 'aerosol radiative
36 forcing' (the perturbation to the earth's radiation budget caused by the presence of aerosols).
37 Positive forcing implies atmospheric warming and vice-versa. (Liao and Seinfeld, 1998;
38 Podgorny and Ramanathan, 2001; Satheesh, 2002; Johnson et al., 2003; Kim et al., 2004;
39 Moorthy et al., 2004; Meloni et al., 2005; Satheesh and Moorthy, 2005; Seinfeld and Pandis,
40 2006; Satheesh et al., 2008; Chand et al., 2009; Mishra et al., 2015). According to the climate
41 assessment report, the estimation of aerosol radiative forcing (due to anthropogenic aerosols) is a
42 major cause of uncertainty in the estimation of climate sensitivity and therefore presents a
43 significant impediment to climate modelling (IPCC, 2013). The uncertainty is mostly due to the
44 lack of accurate measurement of the scattering and absorbing properties of the aerosols (Cooke
45 and Wilson, 1996; Menon et al., 2002; Chung and Seinfeld, 2002; Bond and Sun, 2005).

46 The Single Scattering Albedo (SSA), (the fraction of the total extinction of radiation

47 attributed to scattering) is used to distinguish the scattering and absorbing properties of aerosols.
48 SSA represents a unique fingerprint of the type of aerosol and its radiative forcing (Hansen et al.,
49 1997; Haywood et al., 1997; Myhre et al., 1998). In general, purely scattering aerosols have SSA
50 value of approximately 1 while highly absorbing aerosols have SSA less than 0.7. However,
51 SSA retrievals lack high certainty (Bond and Bergstrom, 2006; Bond et al., 2013). Uncertainties
52 in SSA retrievals are due to factors such as cloud contamination, instrumentation error and
53 aerosol modification due to atmospheric processes. A small change in SSA can cause the aerosol
54 radiative forcing to change from negative to positive (Hansen et al., 1997; Seinfeld and Pandis,
55 2006). Loeb and Su (2010) performed a radiative perturbation analysis and found that direct
56 aerosol radiative forcing was highly sensitive to small perturbations in SSA under clear-sky and
57 cloudy-sky conditions. A simulation study using Santa Barbara DISORT Radiative Transfer
58 (SBDART) model in the present work (Section 5.3) shows that a change in SSA from 0.8 to 1
59 can induce a change of 4 Wm^{-2} in the top-of-atmosphere (TOA) flux depending on the aerosol
60 type and aerosol layer height (Figure 8). Better SSA retrievals (both in-situ and satellite-based)
61 are required to reduce the uncertainty in SSA for a more accurate estimation of aerosol forcing;
62 particularly over regions influenced by a variety of air masses. There is also a need for accurate
63 spectral aerosol absorption measurements, which is required to validate SSA derived from
64 satellites (Bergstrom et al., 2007).

65 Studies on the various measurements of aerosol light absorption using instruments and their
66 uncertainty evaluation have been performed previously (Horvath, 1993, Heintzenberg et al.,
67 1997; Moosmuller et al., 2009). The different methods of retrieval of SSA, both ground-based
68 and using satellites, are provided in Table 1. Unlike aerosol absorption coefficient, SSA is not
69 measured directly by an instrument. Instead, it is retrieved using lookup tables or estimated using

70 other parameters which are measured or calculated using models.

71 Though these previous studies on ground-based retrievals have brought a fundamental
72 understanding to the estimation of amounts of aerosols / aerosol chemistry, their restricted spatial
73 and temporal extent is a significant limitation. Moreover, these studies have reduced availability
74 of scenes for indirect retrievals. Some techniques are limited due to cloud contamination while
75 others operate only under specific conditions (e.g. presence of sun glint). This presents a need for
76 better SSA retrieval algorithms that overcome the present technical limitations and that can be
77 applied on a global scale. The global extent of observations from satellites has increased the
78 spatial extent of the observations (Kaufman et al., 2002a). Though the satellite-based SSA
79 retrievals have been shown to be extremely successful over the majority of ocean and land
80 regions, they still have a limited success over deserts and ice sheets. Over deserts and ice-sheets,
81 high surface reflectance affects the satellite retrievals in the visible spectrum. To counter this,
82 SSA is retrieved in the UV spectrum (330 nm to 400 nm) over these regions (Torres et al., 1998,
83 2007). In the UV spectrum, the upwelling radiances are highly sensitive to the aerosol absorption
84 and also have a lower influence of surface albedo (Torres et al., 2007). SSA retrieval in UV
85 spectrum hence avoids difficulties encountered over surfaces with high albedo.

86 The quality of OMI SSA retrievals is affected by sub-pixel cloud contamination (due to the
87 larger footprint of size 13km x 24km) and ~~the~~ [uncertainty in the assumption of](#) spectral surface
88 albedo (Torres et al., 2007). To counter the problems and uncertainties in the OMI SSA retrieval
89 (Table 2), Satheesh et al. 2009 used retrievals from multiple satellites. They used combined
90 retrievals from OMI-MODIS since each of these sensors have their own strengths and both fly
91 within ~7-8 minutes of each other in the A-train constellation (Stephens et al., 2002). The better
92 cloud-screened retrieval of AOD from MODIS (Levy et al., 2003; [2013](#)) and the high sensitivity

93 of OMI to aerosol absorption was used to develop a hybrid algorithm to retrieve SSA (Satheesh
94 et al., 2009). The algorithm uses the MODIS AOD as a reference to infer the aerosol layer height
95 and SSA from OMI. This removes any *a priori* assumption made by the OMI algorithm
96 ~~regarding an aerosol model~~ to retrieve ALH along with SSA. The study by Satheesh et al. 2009
97 was performed over the East tropical Atlantic Ocean, the Central tropical Atlantic Ocean and the
98 Arabian Sea for the year 2006. A comparison of the retrieved aerosol height with aircraft
99 measurements showed that OMI-MODIS was more accurate than OMI. Gassó and Torres (2016)
100 performed a detailed analysis of the OMI UV product retrievals over oceans and island sites.
101 They compared the OMI retrieved AOD with MODIS and AERONET (Aerosol Robotic
102 Network) AODs. They also used the OMI-MODIS algorithm for only two particular cases over
103 and near Africa to understand how the assumption of aerosol height and shape affected AOD and
104 SSA retrievals. ~~It was found that w~~ When the actual height from satellite Lidar was used instead
105 of climatological values and when the shape of dust aerosols was assumed to be non-spherical,
106 the retrievals by OMI agreed better with other observations including the original OMI-MODIS
107 method. The OMI-MODIS algorithm has been used in calculating aerosol radiative forcing
108 (Satheesh et al., 2010) over oceanic regions surrounding India and used in retrieving SSA over
109 land (Narasimhan and Satheesh, 2013) as well as used to understand the retrievals of OMI UV
110 products for two particular cases (Gassó and Torres, 2016). However, a detailed analysis of the
111 algorithm on a larger spatial and temporal scale has not been done so far.

112 The current work applies the OMI-MODIS algorithm to retrieve SSA on a global scale. It is
113 applied over the global oceans from 2008-2012. Regional analysis over the Atlantic, the Arabian
114 Sea and the Bay of Bengal are done by incorporating the aerosol layer height and the type of
115 aerosols. After estimating SSA values using the OMI-MODIS algorithm, the present study then

116 uses cruise measurements of SSA from the Integrated Campaign for Aerosols, Gases and
117 Radiation Budget (ICARB) and winter ICARB campaigns over Arabian Sea and Bay of Bengal
118 in 2006 and 2009 to validate the same (Moorthy et al., 2008, 2010).

119 **2. Data**

120 **2.1. OMI**

121 The Ozone Monitoring Instrument (OMI) onboard the Aura satellite was launched in 2004. For
122 OMI measurements two aerosol inversion schemes are used- OMI near UV (OMAERUV)
123 algorithm and the multi-wavelength (OMAERO) algorithm (Torres et al., 2007). The OMAERO
124 algorithm uses 19 wavelengths in the range of 330-500 nm to retrieve corresponding aerosol
125 characteristics. For the present study, we have used the OMAERUV algorithm which uses
126 measurements at two wavelengths 354 nm and 388 nm. The reason behind choosing these
127 wavelengths is the high sensitivity of upwelling radiances to aerosol absorption and the lower
128 influence of surface in measurements due to low reflectance values in the UV region. In addition
129 to this, the wavelengths also have negligible interference from trace gases. This gives a unique
130 advantage of retrieving aerosol properties over ocean and land including arid and semi-arid
131 regions (Torres et al., 1998; 2007).

132 The products derived from the algorithm include AOD, absorption aerosol optical depth
133 (AAOD) and single scattering albedo (SSA). These are derived from pre-computed reflectance
134 values for different aerosol models. Three major types of aerosols have been used - Desert dust,
135 carbonaceous aerosols from biomass burning and background and urban-industrial aerosols.
136 Each type has seven models of SSA. The retrieved products of OMAERUV are sensitive to the
137 aerosol layer height (Torres et al., 1998) and are reported for five discrete aerosol layer heights,
138 i.e., surface (exponential profile), 1.5, 3.0, 6.0, and 10.0 km with latter four following a Gaussian

139 distribution.

140 Due to the high sensitivity of SSA retrieval to the assumption of aerosol height and aerosol
141 type (Torres et al., 2002), the OMI algorithm was improved (Collection 003-PGE V1.4.2, Torres
142 et al., 2013). The climatology of aerosol layer height from CALIPSO (Cloud-Aerosol Lidar and
143 Infrared Pathfinder Satellite Observations) along with carbon monoxide (CO) measurements
144 from AIRS (Atmospheric Infrared Sounder) have helped distinguish carbonaceous aerosols from
145 dust particles. Torres et al. (2013) showed that the combined use of AIRS CO measurements and
146 OMI Aerosol Index (AI) retrievals, helped in identifying the type of absorbing aerosol. Thus,
147 smoke layers were identified when values of AI and CO measurements were high and during
148 events of high AI and low CO values, the aerosols were identified as dust. The AIRS CO
149 measurements were also used to identify large aerosol loading which was otherwise represented
150 as clouds by the OMAERUV algorithm. Using collocated observations of OMI and Cloud-
151 Aerosol Lidar with Orthogonal Polarization (CALIOP), Torres et al. (2013) estimated the height
152 of elevated absorbing aerosols for a 30-month period from July 2006 to December 2008. An
153 effective aerosol layer height was calculated using the CALIOP 1064 nm attenuated backscatter
154 weighted by corresponding altitudes. The 30-month climatology of aerosol height was used in
155 the OMAERUV retrievals which then validated against the AERONET observations (Torres et
156 al., 2013). The results showed that there was an improvement in the retrievals.

157 Since 2007, observations have been affected by an instrumental issue called the *row*
158 *anomaly* which reduces the quality of radiance at all wavelengths (Jethva et al., 2014). Torres et
159 al. (2018) studied the impact of row anomaly on the OMAERUV retrievals by comparing
160 monthly values AOD, SSA and UV aerosol index (UVAI) of two different sets of scattering
161 angles. Over regions dominated by carbonaceous and sulphate aerosols, the agreement between

162 the sets was better than over arid regions dominated by dust aerosols. Differences were also
163 found over cloudy regions. The discrepancies were attributed to the inaccurate representation of
164 scattering effects of dust aerosols and cloud droplets. Better representation of scattering by
165 clouds and the non-spherical (spheroidal) shape assumption of dust aerosols was found to reduce
166 the inconsistencies in aerosol products due to row anomaly. These improvements have been
167 incorporated in the latest version of OMAERUV product (version 1.8.9) which has been used in
168 the present study. Along with the aerosol products retrieved at different heights, the final set of
169 AOD/SSA/AAOD retrievals in the OMAERUV product is reported at the mean ALH provided
170 by the 30-month long averaged climatology developed using OMI-CALIOP combined
171 observations (Torres et al., 2013). The original aerosol height assumptions were used in the
172 algorithm over regions where the climatology was unavailable.

173 **2.2. MODIS**

174 The Moderate Resolution Imaging Spectrometer (MODIS) instrument on the Aqua satellite
175 was launched in 2002. This instrument, with 36 spectral channels has a unique ability to retrieve
176 aerosol properties with better accuracy over both land and ocean (Remer et al., 2005; Levy et al.,
177 2003). Of these, seven channels (0.47-2.13 μm) are used to retrieve aerosol properties over the
178 ocean (Tanré et al., 1997).

179 As described in Remer et al., (2005), before the retrieval algorithm, masking of sediments,
180 clouds and ocean glint is performed to separate valid pixels from bad ones. The retrieval
181 algorithm of MODIS (also called the inversion procedure) has been described in detail
182 previously (Tanré et al., 1997; Levy et al., 2003; Remer et al., 2005). The algorithm uses a ‘look-
183 up table’ (LUT) approach, i.e., for a set of aerosol and surface parameters, radiative transfer
184 calculations are performed. Spectral reflectance derived from the LUT is compared with

185 MODIS-measured spectral reflectance to find the ‘best’ (least-squares) fit. The resulting
186 combination of modes provides the aerosol model from which size distribution, properties
187 including spectral optical depth, effective radius ~~ete.~~ are derived. The product used from MODIS
188 is the Level 2 aerosol (MYD04, Collection 5.1) product. The parameter chosen is
189 'Effective_Optical_Depth_Average_Ocean' which provides the aerosol optical depth over the
190 ocean at seven wavelengths. The value is the average of all the solutions in the inversion
191 procedure with the least-square error < 3%.

192 A combination of OMI and MODIS helps indirectly in counteracting the cloud
193 contamination problem and also uses the strength of the individual sensors – OMI's sensitivity to
194 aerosol absorption combined with the better cloud screening of MODIS and accurate retrieval of
195 AOD, and aerosol size (Satheesh et al., 2009; Narasimhan and Satheesh, 2013).

196 **3. Algorithm**

197 MODIS aerosol product reports retrievals at 10 x 10 km spatial resolution at nadir (and a cloud
198 mask at 500m and 1km resolution) whereas OMI reports at 13 km x 24 km. This results in an
199 OMI pixel being prone to cloud contamination which may result in an overestimation in AOD
200 and SSA (Torres et al., 1998). However, AAOD can be retrieved in the presence of small cloud
201 contamination since there is cancellation of errors (Torres et al., 2007).

202 The high accuracy of size-resolved aerosol retrievals with MODIS is because the over-ocean
203 algorithm employs all seven channels (0.47-2.13 micron) in the inversion enabling better
204 characterization of fine and coarse particles. (Tanré et al., 1997; Remer et al., 2005; Levy et al.,
205 2003). While OMI is highly sensitive to aerosol absorption in the near-UV region, the accuracy
206 in the retrieval of AAOD depends on the aerosol layer height assumption. OMI provides AOD
207 and AAOD at different heights as prescribed by various aerosol types (Torres et al., 2007).

208 The assumption of aerosol layer height in the OMI algorithm constraints the retrievals of
209 AOD and SSA. The approach proposed in Satheesh et al. (2009) used MODIS AOD as an input
210 to the OMI retrieval algorithm; so that the MODIS AOD constraints the OMI inversion so that
211 the OMI inversion is free to infer the aerosol layer height and SSA. Satheesh et al. (2009)
212 extrapolated MODIS AOD from the visible to 388nm and compared the estimated UV AOD with
213 high quality ground-based AERONET observations. The deviation between linearly-extrapolated
214 MODIS AOD and AERONET AOD was more significant at higher AERONET AOD values.
215 This was attributed to the presence of a large number of fine-mode aerosols which caused a
216 nonlinear curvature to the AOD spectral dependence and affected AOD at UV wavelengths.
217 Hence to improve the linear extrapolation, information on the aerosol spectral curvature was also
218 included. This was achieved by using an average regression equation to correct the MODIS AOD
219 (Satheesh et al., 2009; Equation 3). They showed that MODIS AOD could be first linearly
220 extrapolated to 388 nm and then corrected for curvature before being used as input to the OMI
221 retrieval algorithm. The present work uses the same algorithm as proposed by Satheesh et al.
222 (2009) to retrieve SSA over the oceans for the region 60S-60N and 180W-180E from December
223 2007-November 2012. The methodology is described in detail in the following section.

224 **4. Methodology**

225 The AOD for ocean obtained from the Level 2 aerosol product of Aqua-MODIS (MYD04) was
226 used. Using linear extrapolation with spectral curvature correction (Satheesh et al., 2009), AOD
227 at 388 nm (hereafter, AOD_{388}) was calculated from AOD at seven wavelengths ranging from
228 0.47-2.13 μm . OMI provides AOD and SSA for five different aerosol layer heights starting from
229 the surface and at 1.5, 3.0, 6.0 and 10.0km (AOD_{OMI} and SSA_{388}). It also provides the best
230 estimate of SSA calculated based on the CALIOP aerosol layer height climatology (SSA_{OMI}).

231 For the present study, polar regions are not included. ~~and hence~~ Hence pixels from both
232 OMI and MODIS that are outside the 60S-60N and 180W-180E region are excluded. Pixels with
233 invalid or missing values are also excluded. The various parameters extracted from the data were
234 re-gridded onto a uniform grid of $0.5^\circ \times 0.5^\circ$ within the region of study to reduce computation
235 time. For both the satellites, this procedure was repeated for each swath data which were then
236 combined to calculate the daily means.

237 The daily data from collocated MODIS and OMI were utilised in the final algorithm. As
238 mentioned before OMI provides AOD and SSA for five different aerosol layer heights. Using
239 AOD_{388} as the reference, the corresponding aerosol layer height was calculated from the five
240 AOD_{OMI} values through linear interpolation. This height is then used as a reference to find the
241 SSA using interpolation from the set of SSA_{388} values. Finally, this SSA ($SSA_{OMI-MODIS}$), and the
242 best estimate of SSA (SSA_{OMI}) were compared with each other.

243 5. Results

244 The spatial distribution of SSA retrieved using OMI is shown in Fig. 1a. The values are averaged
245 over five years and plotted seasonally.

246 The SSA retrieved using OMI-MODIS algorithm is shown in Fig. 1b.

247 SSA over open oceans is close to 1 due to the presence of a large amount of sea-salt and
248 sulphate. Closer to land, a variety of aerosols are present which results in SSA varying from 0.85
249 to ~1. Over the oceans, separation of ocean colour effects and aerosol concentrations is difficult.
250 Hence the OMI algorithm retrieves when enough absorbing aerosols are present, i.e. $AI \geq 0.8$
251 (Torres et al., 2013). Only pixels whose quality has been assigned as 0 or the highest quality by
252 OMI have been used. The points flagged for row anomaly are also not used in this study. Thus,
253 the retrievals did not cover the entire globe. From Fig.1a it can be seen that majority of the valid

254 SSA retrievals were over major aerosol sources in the world and not over remote oceanic regions
255 like central equatorial Pacific or Antarctic ocean. The major sources include the vast biomass
256 outflow over the Atlantic Ocean from the west coast of Africa, the dust over the Arabian Sea
257 from the arid areas of Arabia & Africa and the dust blown over the Atlantic Ocean from the
258 Sahara. Other regions like the east coast of China, the Bay of Bengal are influenced by a variety
259 of anthropogenic aerosols during different seasons. In the OMI-MODIS algorithm, the aerosol
260 layer height is retrieved through linear interpolation of AOD_{OMI} at five different heights and
261 AOD_{388} as a reference. Linear interpolation was not performed for OMI retrievals which had a
262 missing value at any particular height or if the OMI retrieval was the same at all heights. Such
263 OMI-MODIS values were considered to be invalid. Similarly, if the MODIS AOD was found to
264 be missing or invalid, the corresponding OMI-MODIS retrieval was also considered invalid. This
265 resulted in a reduction in the total number of valid points in OMI-MODIS algorithm when
266 compared to OMI algorithm (Fig. 1b). However, both the algorithms capture the major oceanic
267 regions which are influenced by a large number of aerosols. Gassó and Torres (2016) for a
268 particular day over the North Central Atlantic compared the AOD values retrieved by OMI and
269 MODIS. They compared the difference with the aerosol cloud mask retrieved by MODIS. It was
270 found that while most of the retrievals of OMI screened the cloudy pixels, some of the best
271 quality (flag=0) pixels were found to be cloud contaminated. This they attributed to the coarser
272 pixel size of OMI compared to the smaller pixel size of MODIS cloud product. At higher cloud
273 fraction, OMI retrieved values implying that they can detect aerosol above clouds or the pixels
274 are prone to cloud contamination. Gassó and Torres concluded that only MODIS cloud fraction
275 could not be used to screen out OMI pixels. A larger spatiotemporal scale of such an analysis is
276 required but is beyond the scope of this manuscript and will be addressed in the future. However,

277 OMI retrievals at higher cloud fraction could be the reason for more points in Fig. 1a than OMI
278 MODIS in Fig. 1b.

279 Two important regions over oceans influenced by a variety of aerosols are the tropical
280 Atlantic Ocean and the oceans around the Indian subcontinent. The new approach was used over
281 these regions- Atlantic (5N-30N; 60W-20W) (ATL) and Arabian Sea and Bay of Bengal (0-25N;
282 55E-100E) (ARBOB).

283 **5.1. Difference in SSA retrieval algorithms during different seasons**

284 To understand how the OMI-MODIS algorithm compares with the retrieval using the existing
285 OMI algorithm, the difference between $SSA_{\text{OMI-MODIS}}$ and SSA_{OMI} (ΔSSA) averaged over five
286 years for different seasons is shown in Fig. 2.

287 During March-April May (MAM) and June-July-August (JJA), there is a longitudinal
288 gradient in ΔSSA from the coast of Sahara towards the open Atlantic Ocean. Kaufman et al.
289 (2002a) showed that close to the coast of Africa, aerosols are more absorbing than those away
290 from the coast. The difference in the type of aerosols as we move away from the coast could be
291 one of the reasons for the gradient in ΔSSA . The difference can also be attributed to the shape of
292 dust aerosols which are present in large numbers near the coast of Africa (Torres et al., 2018).
293 The ΔSSA changes sign with season. This was attributed to the change in aerosol layer height
294 and (or) aerosol physical and optical properties.

295 Both ATL and ARBOB regions are influenced by the type of aerosols which result in a
296 complex mixture and eventually resulting in the variation in SSA distribution over each season.
297 While the spatial plot of ΔSSA in Fig. 2 represents the regions where maximum and minimum
298 differences are located around the globe, a distribution plot provides the ranges of ΔSSA which
299 dominate and which do not. The distribution of ΔSSA for different seasons averaged over five

300 years (2008-2012) is plotted in Fig. 3a and 3b for the regions- ATL and ARBOB respectively.

301 Over the tropical Atlantic Ocean, Δ SSA was found within ± 0.03 >80% of the time during
302 all the seasons. Over Arabian Sea and Bay of Bengal, the values of SSA matched within ± 0.03
303 during MAM when dust is present in large quantity over the region. However, Δ SSA has values
304 lower than < -0.03 especially during the seasons of JJA and SON. Satheesh et al. (2009) showed
305 in their analysis that the reason for the discrepancies during non-dust seasons could be due to the
306 wrong assumption of aerosol layer height (ALH) or due to the wrong assumption of aerosol
307 model. Before understanding the role of ALH in SSA retrieval, the meteorological conditions of
308 the ARBOB region (Arabian Sea and Bay of Bengal separately), for different seasons are studied
309 and trajectory analysis is done. This helps in identifying major sources of aerosols during each
310 season.

311 **5.2. Trajectory analysis**

312 **Arabian Sea and Bay of Bengal (ARBOB)**

313 The Arabian Sea and the Bay of Bengal are oceanic regions on the west and east coast of
314 India respectively. Both regions are influenced by various types of aerosols during different
315 seasons. The Arabian Sea has been dominated by dust aerosols and is influenced by high levels
316 of dust during certain seasons as seen from satellite images (Sirocko and Sarnthein, 1989). Pease
317 et al. (1998) studied the geochemistry and the transport of various dust samples during different
318 cruises in different seasons. During winter and summer, the pattern of aerosol transport was
319 similar to that of the Indian monsoon pattern – northeasterly (winter) and southwesterly
320 (summer). Thus, the major sources of aerosols were the Arabian Peninsula (including Saharan
321 dust and the Middle East) and Indian sub-continent in summer and winter respectively. The mean
322 7-day back trajectory using HYSPLIT model from a point over the Arabian Sea (15N; 65E) was

323 performed for each season of 2010 and at three different heights (500m, 1500m and 2500m
324 above MSL). The Arabian Sea region was divided into four quadrants – 1) Arabian Peninsula and
325 North Africa, 2) Central Africa, 3) Indian sub-continent and 4) Indian Ocean and Southeast Asia
326 (Fig. 4). The influence of different aerosol source regions over the Arabian Sea is given in Table
327 2.

328 Similar to Pease et al. (1998), Tindale and Pease (1999) found that transport of aerosols near
329 the surface followed the surface wind currents. The dust content was low near the surface during
330 summer due to the presence of Findlater jet, but the general dust concentrations were higher than
331 other oceanic regions. During winter, the winds are predominantly north and northeasterly and
332 hence results in transport of aerosols from India/Pakistan/Afghanistan onto the Arabian Sea.
333 However, the presence of anticyclonic circulation over Arabia (20N; 60E) results in
334 northwesterly winds transporting dust over the Arabian Sea (Rajeev et al., 2000). The springtime
335 (March-April-May) is the transition between northeast and southwest monsoon. The winds
336 become south westerlies which result in the advection of aerosols from the open Indian Ocean or
337 near Somalia. At higher altitudes (above the Findlater jet) dust transport occurs from Arabia.
338 During summer, the southwest monsoon wind patterns carry aerosols all the way from
339 southeast/east Indian Ocean (mainly sea-salt). As the altitude increases, the wind patterns change
340 a little due to aerosols coming from southwest Indian Ocean/Somalia. Above the Findlater jet, as
341 explained by Tindale and Pease (1999), dust transport occurs from Arabian Peninsula (Table 2).

342 Being an integral part in the Indian Summer Monsoon, studies over the Bay of Bengal is
343 important especially the role of aerosols in the local climate change. While the Arabian Sea is
344 dominated by dust and oceanic aerosols, studies have shown that the Bay of Bengal is influenced
345 by various air masses associated with Asian monsoon system including those of anthropogenic

346 origin (Krishnamurti et al., 1998). The synoptic meteorological conditions over the Bay of
347 Bengal have been studied in detail by Moorthy et al. (2003) and Satheesh et al. (2006). Similar to
348 the other two regions, mean 7-day back trajectory analysis from a point over (15N; 90N) was
349 performed for each season of 2010 and at three different heights (500m, 1500m and 2500m
350 above MSL). The four quadrants representing the various aerosol source regions are 1)
351 India/Arabian Peninsula, 2) Indian Ocean, 3) North/Northeast India and East Asia and 4)
352 Southeast Asia (Fig. 5). Table 3 represents the influence of aerosol source regions over the Bay
353 of Bengal.

354 The northwesterly winds occur from west to east in the Indo-Gangetic Plain (IGP) and due
355 to subsidence, the aerosols are trapped in the east during winter (Dey and Di Girolamo, 2010; Di
356 Girolamo et al., 2004). The IGP with its heavy population and large number of industries acts as
357 a source for anthropogenic aerosols which are transported to Bay of Bengal during winter
358 (Kumar et al., 2013). Along with mineral dust from the Arabian Peninsula, biomass aerosols
359 from Southeast Asia are also transported to the bay. Field experiments like ICARB (Moorthy et
360 al., 2008) during the springtime (pre-monsoon) showed transports of aerosols from the Arabian
361 Peninsula and also the presence of elevated aerosols (anthropogenic and natural) over Bay of
362 Bengal (Satheesh et al., 2008). The post-monsoon season acts as a transition from the summer to
363 winter monsoon. The winds during September are still south westerlies and during October weak
364 westerlies are present (Lawrence and Lelieveld, 2010). This results in transportation of aerosols
365 from the Indian Ocean and the Arabian Sea. Thus, from Table 3 it can be seen that both
366 anthropogenic aerosols (from IGP, Southeast Asia) and natural aerosols (marine and dust) are
367 present over the Bay of Bengal during different seasons.

368 **5.3. Role of Aerosol Layer Height in SSA retrieval**

369 Sathesh et al. (2009) devised a new algorithm to improve the retrieval of SSA using
370 combined OMI and MODIS data. They used MODIS-predicted UV AOD as the input to improve
371 the original OMI algorithm, which was constrained by the assumption of aerosol layer height.
372 Over the Atlantic, they found that on an average the AOD values retrieved from both algorithms
373 agreed within ± 0.1 . However, over the Arabian Sea only when there was considerable loading of
374 dust (especially during the March-April-May season), the OMI AOD and MODIS AOD had
375 agreement suggesting that during other seasons, the assumption of aerosol height could be
376 wrong. Sathesh et al. (2009) also found that over the Arabian Sea the aerosol layer height
377 (ALH) derived from OMI-MODIS algorithm agreed well with aircraft measurements when
378 compared to OMI SSA retrieval. In the current work, the aerosol layer height (ALH) provide by
379 OMI, is the mean climatological height (section 2.1). For OMI-MODIS the ALH is estimated
380 from OMI AOD values (at five different heights) by linear interpolation using AOD_{388} as a
381 reference (section 4). The difference in aerosol layer height (ALH) between OMI-MODIS and
382 OMI was plotted against the difference in SSA over the Arabian Sea and Bay of Bengal (Fig. 6a).
383 The colorbar represents ALH estimated by OMI-MODIS algorithm. The most important
384 observation from this analysis was that OMI overestimated SSA when it overestimated ALH
385 (compared to OMI-MODIS) and vice versa. It has been shown by Gassó and Torres (2016) that
386 when the actual aerosol height measured by Satellite Lidar was 1.5km more than the
387 climatological or assumed height, OMI retrieved higher SSA. It can be seen from Fig. 6a, the
388 blue coloured circles represent height estimated by OMI-MODIS between the surface to ~ 2 km.
389 In this range, it was seen that the height assumed by OMI is > 1.5 km compared to the one
390 estimated by OMI-MODIS. Thus, OMI overestimated SSA compared to the OMI-MODIS
391 retrieval.

392 Gassó and Torres (2016), in their detailed analysis of the OMI UV aerosol product (version
393 1.4.2), studied the OMI-MODIS method for two specific cases. They have mentioned that when
394 the extrapolated MODIS 388nm AOD was not within the OMI LUT values, the OMI-MODIS
395 algorithm retrieves unrealistic height and SSA. For the ARBOB region, the difference in AOD
396 ($AOD_{MODIS} - AOD_{OMI}$) has been plotted with the difference in SSA ($SSA_{OMI-MODIS} - SSA_{OMI}$)
397 (Fig. 6b). The colorbar represents the difference in ALH ($ALH_{OMI-MODIS} - ALH_{OMI}$) retrieved by
398 both the algorithms. An inverse relation was seen implying that when OMI underestimated AOD
399 compared to MODIS, OMI overestimated SSA compared to OMI-MODIS. The difference in
400 AOD was mainly within the ± 0.5 range. However, there are a few points where the AOD
401 difference was > 3 . Mostly in such cases, the difference between the ALH and SSA estimates of
402 both the algorithms was high. However, there are points when the AOD difference was high and
403 the ALH and SSA differences were within ± 1 km and ± 0.03 respectively. Similarly, the
404 difference between ALH and SSA values of both the algorithms was high when the AOD
405 difference was within ± 0.5 . These discrepancies could be attributed to the AOD spectral
406 curvature of an aerosol type assumed by MODIS which is different ~~by~~ from the aerosol model
407 assumed by OMI UV aerosol product (Gassó and Torres, 2016). Whether any other property
408 apart from AOD and shape (for dust aerosols) can affect the ALH and SSA retrievals have to be
409 studied in the future.

410 The importance of ALH and SSA in the calculation of TOA flux was studied using the Santa
411 Barbara DISORT (SBDART) model (Ricchiazzi et al., 1998). For the same tropical environment
412 variables and surface albedo of 0.06, the SSA was varied from 0.8 to 1 and aerosol height from 0
413 to 10 km at 1 km interval. The simulations were done for a narrow band in UV (300-400nm). For
414 a constant AOD, AE (Angstrom Exponent) and asymmetry factor (0.4, 1 and 0.7 respectively),

415 TOA flux was calculated (Fig. 7a). It can be seen that at any ALH, TOA flux varied with SSA.
416 The role of ALH is important in the UV region due to the phenomena of Rayleigh scattering (van
417 de Hulst, 1981). The importance of Rayleigh scattering on the role of ALH is further shown in
418 Fig. 7b. In this particular set of simulations, the Rayleigh scattering is completely removed and
419 all other parameters are kept the same as in Fig. 7a. It can be seen that once molecular scattering
420 is removed, the effect of ALH is also removed and TOA flux depends only on SSA and other
421 aerosol properties. The basis of many aerosol retrievals by satellites in the UV spectrum is the
422 sensitivity of aerosol absorption to Rayleigh scattering which acts as a bright background and
423 contributes to the TOA radiance (Torres et al., 1998; 2002). Change in ALH can affect the TOA
424 radiance since the aerosol layer will interact with the Rayleigh scattering due to molecules
425 present in the atmosphere. However, this effect is smaller compared to the effect due to the
426 change in AOD and SSA (Kim et al., 2018). Kim et al. (2018) also showed how the
427 misclassification of aerosol type and size could affect ALH retrieval. OMI SSA retrievals which
428 are based on LUT depend on the ALH assumed along with aerosol type. The SBDART
429 simulations in the current work show how for a particular TOA flux, SSA varies with ALH when
430 the other aerosol properties are kept constant.

431 **5.4. Comparison between SSA retrievals from OMI and OMI-MODIS with ship-borne** 432 **estimates.**

433 To validate the new retrieval method of SSA using OMI and MODIS, both SSA values from
434 OMI and OMI-MODIS were compared with ground-based measurements (SSA at 450nm)
435 during cruises in the period 2006 and 2009 in the Arabian Sea and Bay of Bengal. These cruises
436 were part of the Integrated Campaign for Aerosols, gases and Radiation Budget (ICARB)
437 performed during the months of March to May 2006 and once during winter (W-ICARB) from

438 27 December 2008 to 30 January 2009 (Moorthy et al., 2008 and 2010). During both the cruises
439 the aerosol sampling was done onboard the Oceanic Research Vessel *Sagar Kanya*. While the
440 2006 cruise covered both the Arabian Sea and the Bay of Bengal, the winter cruise of 2009
441 covered the Bay of Bengal. The cruise tracks are provided in detail in Moorthy et al., 2008 and
442 2010, respectively. The SSA values at different wavelengths were estimated from spectral values
443 of the absorption coefficient and scattering coefficient measured using the instruments
444 Aethalometer (Magee Scientific AE-31, USA) and an integrating nephelometer (TSI 3563, USA)
445 respectively. More details about the instrument and measuring techniques including the
446 uncertainties are provided in Nair et al. (2008). However, both the cruise did not estimate SSA
447 values in the UV spectrum. The closest wavelength at which SSA is calculated is 450nm which
448 has been used to compare with the satellite retrievals of SSA (388nm). Ground-based SSA
449 estimates based on in-situ measurements are seldom consistent with columnar satellite retrievals
450 especially when elevated aerosols are present. This uncertainty along with the uncertainty in the
451 assumption of SSA being uniform between 388nm and 450nm implies that the current
452 comparison of study cannot be used as a validation study. Instead, it is used to understand the
453 consistency of SSA retrievals from satellites with ground-based observations. Since the cruise
454 measurements had little coverage spatially, for better coverage, a 2° box was used around each
455 location within which the mean SSA was calculated for the respective cruise period. These
456 values are plotted in Fig. 8. OMI comparison is given by circles and OMI-MODIS by square
457 markers. It can be seen that despite using a 2° box, the number of points having valid SSA values
458 for the cruise and the satellite retrievals was only 21. This number increased as the size of the
459 box around each cruise location was increased. The low number is due to the sparse nature of the
460 OMI-MODIS retrieval over the region (Fig. 1b). The colour scale represents the cruise and the

461 region where the aerosol sampling was taken.

462 During the ICARB, [the](#) presence of elevated aerosols at a height of ~1km-3km have been
463 shown in earlier studies (Satheesh et al., 2008; Nair et al., 2009). In such cases comparison
464 between a ship-based aerosol retrieval which detects aerosols close to the surface and the SSA
465 retrieval from satellites which detects these elevated aerosols cannot be considered appropriate.
466 This discrepancy was seen in Fig. 8 especially over the Arabian Sea (Blue colour) and some
467 points over Bay of Bengal (Red). In some cases, OMI was able to retrieve SSA consistent with
468 the cruise estimated, unlike OMI-MODIS. This could be due to the improvement of dust model
469 assumption in the new version of OMI aerosol product and (or) due to the wrong spectral AOD
470 dependence assumed by MODIS. During the winter most of the aerosols influencing the Bay of
471 Bengal is present closer to the surface. In such cases comparing the SSA estimates can be valid.
472 It was observed that during winter when aerosols are generally present close to the surface, OMI-
473 MODIS retrieved SSA which is a bit more consistent with the ship estimates compared to OMI.
474 In such cases, OMI still overestimated SSA despite the improvement in the algorithm. The
475 respective RMSEs for OMI and OMI-MODIS comparison with the cruise estimates were 0.05
476 and 0.06. Due to the lack of common points, the correlation was also poor (OMI-MODIS: 0.11
477 and OMI: -0.35).

478

479 The OMI-MODIS approach in SSA retrieval is one of the many combinations of sensors that
480 can be used in retrieving aerosol properties. A better approach involving the vertical distribution
481 of aerosols either from space or ground-based observations is required to reduce the uncertainty
482 further. However, with few ground-based measurements in the UV regime especially over the
483 oceans and fewer retrievals of the vertical aerosol absorption, validation of new algorithms is

484 still in the nascent stage.

485 **6. Summary and Conclusions**

486 Aerosol forcing depends on aerosol properties ~~like such as~~ aerosol optical depth (AOD) and
487 single scattering albedo (SSA). SSA is highly sensitive to the aerosol composition ~~and~~, size and
488 ~~as well as~~ the wavelength at which the aerosol interacts with radiation. A slight change in SSA
489 value can alter the sign of the forcing. Hence it is important to have an accurate measurement of
490 SSA globally. The Ozone Monitoring Instrument (OMI) retrieves SSA in the UV spectrum.
491 However, these retrievals might be affected by the cloud contamination due to the coarser pixel
492 resolution of 13 x 24 km² ~~are affected by cloud contamination~~ and are sensitive to the
493 assumption of aerosol layer height in the inversion procedure. In addition to these problems,
494 uncertainty in the surface albedo is a source of error for SSA retrieval. To resolve the issue of
495 sub-pixel cloud contamination, Satheesh et al. (2009) developed a method using the combination
496 of OMI and the Moderate Resolution Imaging Spectroradiometer (MODIS) at a local scale. In
497 the present study, we used the method developed by Satheesh et al. (2009) to retrieve SSA at a
498 much larger spatial and temporal scales. The main findings from our study are listed below:

- 499 1. Both OMI and OMI-MODIS algorithms retrieved SSA over regions influenced by large
500 amounts of aerosols with moderate to high absorption capacity (e.g. Atlantic Ocean –
501 ATL; Arabian Sea and Bay of Bengal – ARBOB)
- 502 2. The difference in SSA retrievals of both the algorithms (Δ SSA) was found to be within
503 ± 0.03 over ATL >for more than 80% of the time during all the seasons. Over the Arabian
504 Sea, as seen in Satheesh et al. (2009), Δ SSA was within the ± 0.03 range during MAM
505 when the region was influenced by dust. The discrepancy during other season was due to
506 the wrong assumption of aerosol layer height by OMI. The discrepancy in SSA could

507 [also be partly attributed to the sub-pixel cloud contamination during the summer](#)
508 [monsoon season.](#)

509 3. From Fig. 6a it was seen that OMI overestimated SSA when it overestimated ALH and
510 vice versa. This could be attributed to the wrong assumption of aerosol height. Fig. 6b
511 showed that difference in AOD and difference in SSA had an inverse relationship.
512 Further analysis on whether any other factor apart from ALH and aerosol shape can affect
513 SSA retrieval has to be studied.

514 4. Both SSA retrievals were compared with cruise data from the ICARB and W-ICARB
515 campaigns in the Arabian Sea and Bay of Bengal.

516 5. While both the algorithms did not match the cruise estimate during most of the dust
517 season due to the presence of elevated aerosols [not sampled by surface instrument](#), in few
518 cases during ICARB, OMI performed better than OMI-MODIS. This could be due to the
519 better assumption of dust model in the algorithm and/or wrong model assumption by
520 MODIS. During winter, when the aerosols were present closer to the surface, OMI-
521 MODIS was a bit more consistent compared to OMI. This may be due to scenarios where
522 the CALIPSO climatology was absent and OMI used its previous aerosol model
523 assumptions. This could also be due to uncertainties in ALH value even after the
524 improvement in the OMI algorithm with the addition of CALIPSO climatology.

525 OMI retrieves aerosol properties at high cloud fraction (Gassó and Torres, 2016) implying
526 two things, either OMI is able to detect aerosols present above clouds or the OMI pixel was
527 prone to cloud contamination. In their study, Gassó and Torres (2016), observed that while
528 MODIS cloud fraction could be used to screen out cloudy pixels in OMI, it could not be the lone
529 criterion. While they performed for a single case, an analysis of a larger spatial and temporal

530 scale is required. Aerosol type and aerosol layer height play a vital role in the retrieval of aerosol
531 properties. Without the assumption of aerosol type or height, OMI-MODIS provided SSA
532 retrievals which was consistent with cruise estimates during the winter when the Bay of Bengal
533 was influenced by anthropogenic aerosols present close to the surface. This was not the case
534 when dust aerosols were present. This discrepancy can be attributed to the difference in the
535 aerosol model assumption by MODIS and OMI. This comparison study had very few points for a
536 detailed analysis. Hence, an accurate comparison and validation of such retrieval algorithms can
537 be possible only when there are more ground-based observations available in the UV spectrum
538 on a larger spatial and temporal scale along with vertical profiles of aerosol absorption.

539 **Acknowledgements**

540 The authors gratefully acknowledge the NOAA Air Resources Laboratory (ARL) for the
541 provision of the HYSPLIT transport and dispersion model used in this publication. The authors
542 are grateful to NASA data and services centre.

543 **References**

- 544 Bergstrom, R.W., Pilewskie, P., Russell, P.B., Redemann, J., Bond, T.C., Quinn, P.K., and Sierau,
545 B.: Spectral absorption properties of atmospheric aerosols, *Atmos. Chem. Phys.*, 7, 5937-
546 5943, 2007.
- 547 Bond, T.C., and Sun, H.: Can reducing black carbon emissions counteract global warming?,
548 *Environ. Sci. Technol.*, 39(16), 5921-5926, 2005.
- 549 Bond, T.C., and Bergstrom, R.W.: Light absorption by carbonaceous particles: An investigative
550 review, *Aerosol Sci. Tech.*, 40(1), 27-67, doi:10.1080/02786820500421521, 2006.
- 551 Bond, T.C., Doherty, S.J., Fahey, D.W., Forster, P.M., Bernsten, T., De Angelo, B.J., Flanner,
552 M.G., Ghan, S., Karcher, B., Koch, D., Kinne, S., Kondo, Y., Quinn, P.K., Sarofim, M.C.,

553 Schultz, M., Venkataraman, C., Zhang, H., Zhang, S., Bellouin, N., Guttikunda, S.K.,
554 Hopke, P.K., Jacobson, M.Z., Kaiser, J.W., Klimont, Z., Lohmann, U., Schwarz, J.P.,
555 Shindell, D., Storelvmo, T., Warren, S.G., and Zender, C.S.: Bounding the role of black
556 carbon in the climate system: A scientific assessment, *J. Geophys. Res.*, 118(11), 5380-
557 5552, doi:10.1002/jgrd.50171, 2013.

558 Chand, D., Wood, R., Anderson, T.L., Satheesh, S.K., and Charlson, R.J.: Satellite-derived direct
559 radiative effect of aerosols dependent on cloud cover, *Nat. Geosci.*, 2, 181–184,
560 doi:10.1038/ngeo437, 2009.

561 Chung, S.H., and Seinfeld, J.H.: Global distribution and climate forcing of carbonaceous
562 aerosols, *J. Geophys. Res.*, 107(D19), 4407, doi:10.1029/2001JD001397, 2002.

563 Cooke, W.F., and Wilson, J.J.N.: A global black carbon aerosol model, *J. Geophys. Res.*, 101,
564 19395-19410, doi:10.1029/96JD00671, 1996.

565 Dey, S., and Di Girolamo, L.: A climatology of aerosol optical and microphysical properties over
566 the Indian subcontinent from 9 years (2000–2008) of Multiangle Imaging
567 Spectroradiometer (MISR) data, *J. Geophys. Res.*, 115, D15204,
568 doi:10.1029/2009JD013395, 2010.

569 Di Girolamo, L., Bond, T.C., Bramer, D., Diner, D.J., Fettingner, F., Kahn, R.A., Mrtonchik, J.V.,
570 Ramana, M.V., Ramanathan, V., and Rasch, P.J.: Analysis of Multi-angle Imaging
571 SpectroRadiometer (MISR) aerosol optical depths over greater India during winter 2001-
572 2004, *Geophys. Res. Lett.*, 31(23), L23115, doi:10.1029/2004GL021273, 2004.

573 Diner, D.J., Beckert, J.C., Reilly, T.H., Bruegge, C.J., Conel, J.E., Kahn, R.A., Martonchik, J.V.,
574 Ackerman, T.P., Davies, R., Gerstl, S.A.W., Gordon, H.R., Muller, J.-P., Myneni, R.B.,
575 Sellers, P.J., Pinty, B., and Verstraete, M.M.: Multi-angle Imaging SpectroRadiometer

576 (MISR) instrument description and experiment overview, *IEEE T GEOSCI REMOTE*,
577 36(4), 1072-1087, doi:10.1109/36.700992, 1998.

578 Dubovik, O., and King, M.D.: A flexible inversion algorithm for retrieval of aerosol optical
579 properties from Sun and sky radiance measurements, *J. Geophys. Res.*, 105(D16), 20673-
580 20696, doi:10.1029/2000JD900282, 2000.

581 Dubovik, O., Holben, B.N., Eck, F.T., Smirnov, A., Kaufman, Y.J., King, M.D., Tanré, D., and
582 Slutsker, I.: Variability of absorption and optical properties of key aerosol types observed
583 in worldwide locations, *J. Atmos. Sci.*, 59(3), 590-608, doi:10.1175/1520-
584 0469(2002)059<0590:VOAAOP>2.0.CO;2, 2002.

585 Eck, T.F., Holben, B.N., Slutsker, I., and Setzer, A.: Measurements of irradiance attenuation and
586 estimation of aerosol single scattering albedo for biomass burning aerosols in Amazonia, *J.*
587 *Geophys. Res.*, 103(D24), 31865-31878, doi:10.1029/98JD00399, 1998.

588 Gassó, S., and Torres, O.: The role of cloud contamination, aerosol layer height and aerosol
589 model in the assessment of the OMI near-UV retrievals over the ocean, *Atmos. Meas.*
590 *Tech.*, 9, 3031-3052, doi:10.5194/amt-9-3031-2016, 2016.

591 Hansen, J., Sato, M., and Ruedy, R.: Radiative forcing and climate response, *J. Geophys. Res.-*
592 *Atmos.*, 102(D6), 6831-6864, doi:10.1029/96JD03436, 1997.

593 Harriss, R.C., Browell, E.V., Sebacher, D.I., Gregory, G.L., Hinton, R.R., Beck, S.M., McDougal,
594 D.S., and Shipley, S.T.: Atmospheric transport of pollutants from North America to the
595 North Atlantic Ocean, *Nature*, 308, 722-724, doi:10.1038/308722a0, 1984.

596 Haywood, J.M., Roberts, D.L., Slingo, A., Edwards, J.M., and Shine, K.P.: General circulation
597 model calculations of the direct radiative forcing by anthropogenic sulphate and fossil-fuel
598 soot aerosol, *J. Clim.*, 10, 1562-1577, doi:10.1175/1520-

599 0442(1997)010<1562:GCMCOT>2.0.CO;2, 1997.

600 Heintzenberg, J., Charlson, R.J., Clarke, A. D., Liousse, C., Ramaswamy, V., Shine, K.P.,
601 Wendish, M., and Helas, G.: Measurements and modelling of aerosol single-scattering
602 albedo: Progress, problems and prospects, *Contrib. Atmos. Phys.*, 70(4), 249– 263, 1997.

603 Herman, B.M., Browning, R.S., and De Luisi, J.J.: Determination of the effective imaginary term
604 of the complex refractive index of atmospheric dust by remote sensing: the diffuse-direct
605 radiation method, *J. Atmos. Sci.*, 32, 918-925, doi:10.1175/1520-
606 0469(1975)032<0918:DOTEIT>2.0.CO;2, 1975.

607 Herman, J.R., Bhartia, P.K., Torres, O., Hsu, C., Seftor, C., and Celarier, E.: Global distribution
608 of UV-absorbing aerosols from Nimbus 7/TOMS data, *J. Geophys. Res.-Atmos.*, 102(D14),
609 16911-16922, doi:10.1029/96JD03680, 1997.

610 Horvath, H.: Atmospheric light absorption- a review, *Atmos. Environ. A-Gen.*, 27(3), 293-317,
611 doi:10.1016/0960-1686(93)90104-7, 1993.

612 Intergovernmental Panel on Climate Change (IPCC) (2013), The physical science basis:
613 Contribution of Working Group I to the Fifth Assessment Report of the Intergovernmental
614 Panel on Climate Change, In: *Climate Change (2013)*, Stocker, T.F., D. Qin, G.K. Plattner,
615 M. Tignor, S.K. Allen, J. Boschung, A. Nauels, Y. Xia, V. Bex, and P.M. Midgley (eds),
616 Cambridge University, Press: Cambridge, United Kingdom and New York, NY, USA 1535
617 pp, doi:10.1017/CBO9781107415324.

618 Jethva, H., Torres O., and Ahn C.: Global assessment of OMI aerosol single-scattering albedo
619 using ground-based AERONET inversion, *J. Geophys. Res.-Atmos.*, 119(14), 9020-9040,
620 doi:10.1002/2014JD021672, 2014.

621 Johnson, B.T., Shine, K.P., and Forster, P.M.: The semi-direct aerosol effect: Impact of absorbing

622 aerosols on marine stratocumulus, *Q. J. Roy. Meteor. Soc.*, 130, 1407-1422,
623 doi:10.1256/qj.03.61, 2003.

624 Kaufman, Y.J.: Satellite sensing of aerosol absorption, *J. Geophys. Res.*, 92, 4307-4317,
625 doi:10.1029/JD092iD04p04307, 1987.

626 Kaufman, Y.J., Tanré, D., and Boucher, O.: A satellite view of aerosols in the climate system,
627 *Nature*, 419, 215-223, doi:10.1038/nature01091, 2002a.

628 Kaufman, Y.J., Martins, J.V., Remer, L.A., Schoeberl, M.R., and Yamasoe, M.A.: Satellite
629 retrieval of aerosol absorption over the oceans using sunglint, *Geophys. Res. Lett.*, 29(19),
630 34-1 – 34-4, doi:10.1029/2002GL015403, 2002b.

631 Kaufman, Y.J., Koren, I., Remer, L.A., Tanré, D., Ginoux, P., and Fan, S.: Dust transport and
632 deposition observed from the Terra-Moderate Resolution Imaging Spectroradiometer
633 (MODIS) spacecraft over the Atlantic Ocean, *J. Geophys. Res.*, 110, D10S12,
634 doi:10.1029/2003JD004436, 2005.

635 Kim, S-W., Yoon, S-C., Jefferson, A., Won, J-G, Dutton, E.G, Ogren, J.A., and Anderson T.L.:
636 Observation of enhanced water vapour in Asian dust layer and its effect on atmospheric
637 radiative heating rates, *Geophys. Res. Lett.*, 31(18), doi:10.1029/2004GL020024, 2004.

638 Kim, M., Kim, J., Torres, O., Ahn, C., Kim, W., Jeong, U., Go, S., Liu X., Moon, K.J., and Kim,
639 D.-R.: Optimal Estimation-Based Algorithm to Retrieve Aerosol Optical Properties for
640 GEMS Measurements over Asia, *Remote Sens.*, 10(2), 162, doi:10.3390/rs10020162, 2018.

641 King, M.D.: Determination of the ground albedo and the index of absorption of atmospheric
642 particulates by remote sensing. Part II: Application, *J. Atmos. Sci.*, 36, 1072-1083,
643 doi:10.1175/1520-0469(1979)036<1072:DOTGAA>2.0.CO;2, 1979.

644 Krishnamurti, T.N., Jha, B., Prospero J., Jayaraman, A., and Ramanathan, V.: Aerosol and

645 pollutant transport and their impact on radiative forcing over the tropical Indian Ocean
646 during the January – February 1996 pre-INDOEX cruise, *Tellus B*, 50(5): 521–542,
647 doi:10.1034/j.1600-0889.1998.00009.x, 1998.

648 Kumar, K.R., Sivakumar, Reddy, R.R., and Gopal, K.R.: Ship-borne measurements of columnar
649 and surface aerosol loading over the Bay of Bengal during W-ICARB campaign: role of
650 airmass transport. *Latitudinal and Longitudinal Gradients, Aerosol Air Qual Res.*, 13, 818–
651 837, doi:10.4209/aaqr.2012.08.0225, 2013.

652 Lawrence, M.G., and Lelieveld, J.: Atmospheric pollutant outflow from southern Asia: a review,
653 *Atmospheric Chemistry and Physics*, 10, 11017-11096, doi:10.5194/acp-10-11017-2010,
654 2010.

655 Levy, R.C., Remer, L.A., Tanré, D., Kaufman, Y.J., Ichoku, C., Holben, B.N., Livingston, J.M.,
656 Russell, P.B., and Maring, H.: Evaluation of the Moderate-Resolution Imaging
657 Spectroradiometer (MODIS) retrievals of dust aerosol over the ocean during PRIDE, *J.*
658 *Geophys. Res.*, 108(D19), 8594, doi:10.1029/2002JD002460, 2003.

659 [Levy, R.C., Mattoo, S., Munchak, L.A., Remer, L.A., Sayer, A.M., Patadia, F., and Hsu N.C.:](#)
660 [The collection 6 MODIS aerosol products over land and ocean, *Atm. Meas. Tech.*, 6, 2989-](#)
661 [3034, doi:10.5194/amt-6-2989-2013, 2013.](#)

662 Liao, H., and Seinfeld, J.H.: Radiative forcing by mineral dust aerosols: Sensitivity to key
663 variables, *J. Geophys. Res.-Atmos.*, 103(D24), 31637-31645, doi:10.1029/1998JD200036,
664 1998.

665 Meloni, D., di Sarra, A., di Lorio, T., and Fiocco, G: Influence of the vertical profile of Saharan
666 dust on the visible direct radiative forcing, *J. Quant. Spectrosc. Ra.*, 93(4), 397-413,
667 doi:10.1016/j.jqsrt.2004.08.035, 2005.

668 Menon, S., Hansen, J., Nazarenko, L., and Luo, Y.: Climate effects of black carbon aerosols in
669 China and India, *Science*, 297(5590), 2250-2253, doi:10.1126/science.1075159, 2002.

670 Mishra, A.K., Koren, I., and Rudich, Y.: Effect of aerosol vertical distribution on aerosol-
671 radiation interaction: A theoretical prospect, *Heliyon*, e00036,
672 doi:10.1016/j.heliyon.2015.e00036, 2015.

673 Moorthy, K.K., Babu, S.S., and Satheesh, S.K.: Aerosol spectral optical depths over the Bay of
674 Bengal: role of transport, *Geophys. Res. Lett.*, 30(5): 1249, doi:10.1029/2002GL016520,
675 2003.

676 Moorthy, K.K., Babu, S.S., Sunilkumar, S.V., Gupta, P.K., and Gera, B.S.: Altitude profiles of
677 aerosol BC, derived from aircraft measurements over an inland urban location in India,
678 *Geophys. Res. Lett.*, 31(22), 10.1029/2004GL021336, 2004.

679 Moorthy, K.K., Satheesh, S.K., Babu, S.S., and Dutt, C.B.S.: Integrated campaign for aerosols,
680 gases and radiation budget (ICARB): an overview, *J. Earth. Syst. Sci.*, 117(1), 243-262,
681 doi:10.1007/s12040-008-0029-7, 2008.

682 Moorthy, K.K., Beegum, S.N., Babu, S.S., Smirnov, A., John, S.R., Kumar, K.R., Narasimhulu,
683 K., Dutt, C.B.S., and Nair, V.S.: Optical and physical characteristics of Bay of Bengal
684 aerosols during W-ICARB: spatial and vertical heterogeneities in the marine atmospheric
685 boundary layer and in the vertical column, *J. Geophys. Res.*, 115(D24): D24213,
686 doi:10.1029/2010JD014094, 2010.

687 Moosmuller, H., Chakrabarty, R.K., and Arnott, W.P.: Aerosol light absorption and its
688 measurement: A review, *J. Quant. Spectrosc. Ra.*, 110(11), 844-878,
689 doi:10.1016/j.jqsrt.2009.02.035, 2009.

690 Morris, V., Colon, P.C., Nalli, N.R., Joseph, E., Armstrong, R.A., Detres, Y., Goldberg, M.D.,

691 Minnett, P.J., and Lumpkin, R.: Measuring Trans-Atlantic aerosol transport from Africa,
692 EOS Trans. AGU, 87(50), 565-571, doi:10.1029/2006EO500001, 2006.

693 Myhre, G., Stordal, F., Restad, K., and Isaksen, I.S.A.: Estimation of the direct radiative forcing
694 due to sulphate and soot aerosols, *Tellus*, 50B, 463-477, 1998.

695 Nair, V.S., Babu, S.S., and Moorthy, K.K.: Spatial distribution and spectral characteristics of
696 aerosol single scattering albedo over the Bay of Bengal inferred from shipborne
697 measurements, *Geophys. Res. Lett.*, 35, doi:10.1029/2008GL033687, 2008.

698 Nair V.S., Moorthy, K.K., and Babu, S.S.: Optical and Physical Properties of Atmospheric
699 Aerosols over the Bay of Bengal during ICARB, *J. Atmos. Sci.*, 66, doi:
700 10.1175/2009JAS3032.1, 2009.

701 Narasimhan, D., and Satheesh, S.K.: Estimates of aerosol absorption over India using multi-
702 satellite retrieval, *Ann. Geophys.*, 31, 1773-1778, doi:10.5194/angeo-31-1773-2013, 2013.

703 Pease, P.P., Tchakerian, V.P., and Tindale, N.W.: Aerosols over the Arabian Sea: geochemistry
704 and source areas for Aeolian desert dust, *J. Arid Environ.*, 39(3), 477-496,
705 doi:10.1006/jare.1997.0368, 1998.

706 Podgorny, I.A., and Ramanathan, V.: A modeling study of the direct effect of aerosols over the
707 tropical Indian Ocean, *J. Geophys. Res.*, 106(D20): 24097–24105,
708 doi:10.1029/2001JD900214, 2001.

709 Prospero, J.M., and Carlson, T.N.: Vertical and areal distribution of Saharan dust over the
710 western equatorial north Atlantic Ocean, *J. Geophys. Res.*, 77(27), 5255-5265,
711 doi:10.1029/JC077i027p05255, 1972.

712 Prospero, J.M.: Saharan dust transport over the North Atlantic Ocean and Mediterranean: An
713 overview, In: *The Impact of Desert Dust Across the Mediterranean*, Guerzoni S., Chester

714 R. (Eds.), 133-151, doi:10.1007/978-94-017-3354-0_13, 1996.

715 Rajeev, K., Ramanathan, V., and Meywerk, J.: Regional aerosol distribution and its long-range
716 transport over the Indian Ocean, *J. Geophys. Res.-Atmos.*, 105(D2), 2029-2043,
717 doi:10.1029/1999JD900414, 2000.

718 Ramanathan, V., Crutzen, P.J., Kiehl, J.T., and Rosenfield, D.: Aerosols, climate and the
719 hydrological cycle, *Science*, 294(5549): 2119–2124, doi:10.1126/science.1064034, 2001.

720 Remer, L. A., Kaufman, Y. J., Tanré, D., Mattoo, S., Chu, D. A., Martins, J. V., Li, R. R., Ichoku,
721 C., Levy, R. C., Kleidman, R. G., Eck, T. F., Vermote, E., and Holben, B. N.: The MODIS
722 aerosol algorithm, products, and validation, *J. Atmos. Sci.*, 62, 947–973,
723 doi:10.1175/JAS3385.1, 2005.

724 Ricchiazzi, P., Yang, S., Gautier, C., and Sowle, D.: SBDART: a research and teaching software
725 tool for plane-parallel radiative transfer in the earth's atmosphere, *B. Am. Meteorol. Soc.*
726 79(10): 2101–2114, doi:10.1175/1520-0477(1998)079<2101: SARATS>2.0.CO;2, 1998.

727 Satheesh, S.K.: Aerosols and climate, *Resonance*, 7(4), 48-59, doi:10.1007/BF02836138, 2002.

728 Satheesh, S.K., and Moorthy, K.K.: Radiative effects of natural aerosols: a review, *Atmos.*
729 *Environ.*, 39(11): 2089–2110, doi:10.1016/j.atmosenv.2004.12.029, 2005.

730 Satheesh, S.K., Srinivasan, J., and Moorthy, K.K.: Spatial and temporal heterogeneity in aerosol
731 properties and radiative forcing over Bay of Bengal: Sources and role of aerosol transport,
732 *J. Geophys. Res.*, 111(D8): D08202, doi:10.1029/2005JD006374, 2006.

733 Satheesh, S.K., Moorthy, K.K., Babu, S.S., Vinoj, V., and Dutt, C.B.S.: Climate implications of
734 large warming by elevated aerosol over India, *Geophys. Res. Lett.*, 35(19),
735 doi:10.1029/2008GL034944, 2008.

736 Satheesh, S.K., Torres, O., Remer, L.A., Babu, S.S., Vinoj, V., Eck, T.F., Kleidman, R.G., and

737 Holben, B.N.: Improved assessment of aerosol absorption using OMI-MODIS joint
738 retrieval, *J. Geophys. Res.*, 114, D05209, doi:10.1029/2008JD011024, 2009.

739 Satheesh, S.K., Vinoj, V., and Moorthy, K.K.: Assessment of aerosol radiative impact over
740 oceanic regions adjacent to Indian subcontinent using multi-satellite analysis, *Adv.*
741 *Meteorol.*, 2010, Article ID 139186, pp 13., doi:10.1155/2010/139186, 2010.

742 Seinfeld, J.H., and Pandis, S.N.: *Atmospheric Chemistry and Physics: From air pollution to*
743 *climate change*, 2nd Ed., 1232 pp, John Wiley & Sons, Inc., Hobkoben, New Jersey, 2006.

744 Sirocko, F., and Sarnthein, M.: Wind-borne deposits in the northwestern Indian Ocean: Record of
745 Holocene sediments versus modern satellite data, In: *Paleoclimatology and*
746 *Paleometeorology: modern and past patterns of global atmospheric transport*, Leinen M.,
747 Sarnthein M. (Eds), 401-433, Amsterdam: Kluwer Academic Publishers, 1989.

748 Stephens, G.L., Vane, D.G., Boain, R.J., Mace, G.G., Sassen, K., Wang, Z., Illingworth, A.J.,
749 O'Connor, E.J., Rossow, W.B., Durden, S.L., Miller, S.D., Austin, R.T., Benedetti, A.,
750 Mitrescu, C., and CloudSat Science Team: The CloudSat mission and the A-Train: A new
751 dimension of space-based observations of clouds, precipitation, *B. Am. Meteorol. Soc.*, 83,
752 1771-1790, doi:10.1175/BAMS-83-12-1771, 2002.

753 Tanré, D., Kaufman, Y.J., Herman, M., and Mattoo, S.: Remote sensing of aerosol properties
754 over oceans using the MODIS/EOS spectral radiances, *J. Geophys. Res.*, 102(D14),
755 16971–16988, 1997.

756 Tindale, N.W., and Pease, P.P.: Aerosols over the Arabian Sea: Atmospheric transport pathways
757 and concentrations of dust and sea salt, *Deep-Sea Res. Pt. II*, 46(8-9), 1577-1595,
758 doi:10.1016/S0967-0645(99)00036-3, 1999.

759 Torres, O., Bhartia, P. K., Herman, J. R., and Ahmad, Z.: Derivation of aerosol properties from

760 satellite measurements of backscattered ultraviolet radiation. Theoretical Basis, J.
761 Geophys. Res., 103(D14), 17099–17110, 1998.

762 Torres, O., Decae, R., Veefkind, J.P., and de Leeuw, G.: OMI aerosol retrieval algorithm, in OMI
763 Algorithm Theoretical Basis Document: Clouds, Aerosols, and Surface UV Irradiance, 3,
764 V2, OMIATBD- 03, edited by P. Stammes, pp. 47 – 71, NASA Goddard Space Flight
765 Cent., Greenbelt, Md, 2002.
766 ([http://eosps0.gsfc.nasa.gov/eos_homepage/for_scientists/atbd/docs/OMI/ATBD-OMI-](http://eosps0.gsfc.nasa.gov/eos_homepage/for_scientists/atbd/docs/OMI/ATBD-OMI-03.pdf)
767 [03.pdf](http://eosps0.gsfc.nasa.gov/eos_homepage/for_scientists/atbd/docs/OMI/ATBD-OMI-03.pdf))

768 Torres, O., Bhartia, P.K., Sinyuk, A., Welton, E.J., and Holben, B.: Total Ozone Mapping
769 Spectrometer measurements of aerosol absorption from space: Comparison to SAFARI
770 2000 ground-based observations, J. Geophys. Res., 110(D10), doi:10.1029/2004JD004611,
771 2005.

772 Torres, O., Tanskanen, A., Veihelmann, B., Ahn, C., Braak, R., Bhartia, P.K., Veefkind, P., and
773 Levelt, P.: Aerosols and surface UV products from Ozone Monitoring Instrument
774 observations: An overview, J. Geophys. Res., 112, D24S47, doi:10.1029/2007JD008809,
775 2007.

776 Torres, O., Ahn, C., and Chen, Z.: Improvements to the OMI near-UV aerosol algorithm using A-
777 train CALIOP and AIRS observations, Atmos. Meas. Tech., 6, 3257-3270,
778 doi:10.5194/amt-6-3257-2013, 2013.

779 Torres, O., Bhartia, P.K., Jethva, H., and Ahn, C.: Impact of the ozone monitoring instrument row
780 anomaly on the long-term record of aerosol products, Atmos. Meas. Tech., 11, 2701-2715,
781 doi:10.5194/amt-11-2701-2018, 2018.

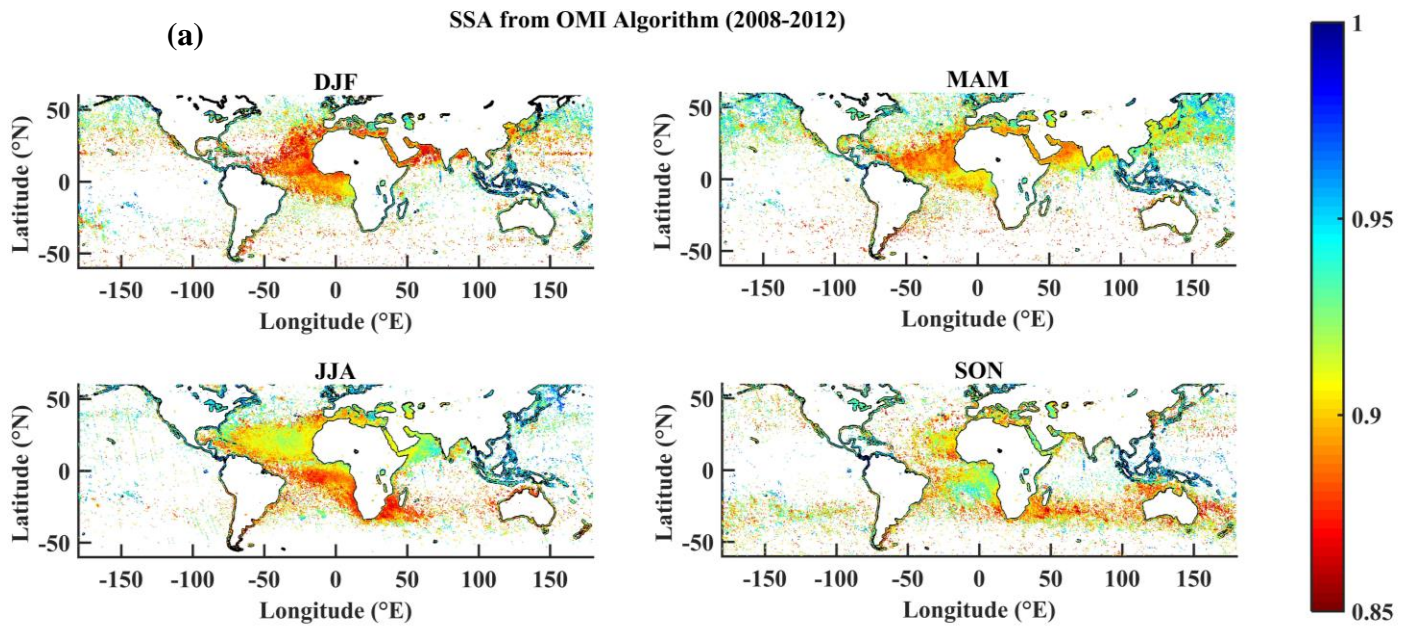
782 Van de Hulst, H.C.: Light scattering by small particles, 496 pp., Dover publications, New York,

783 1981.

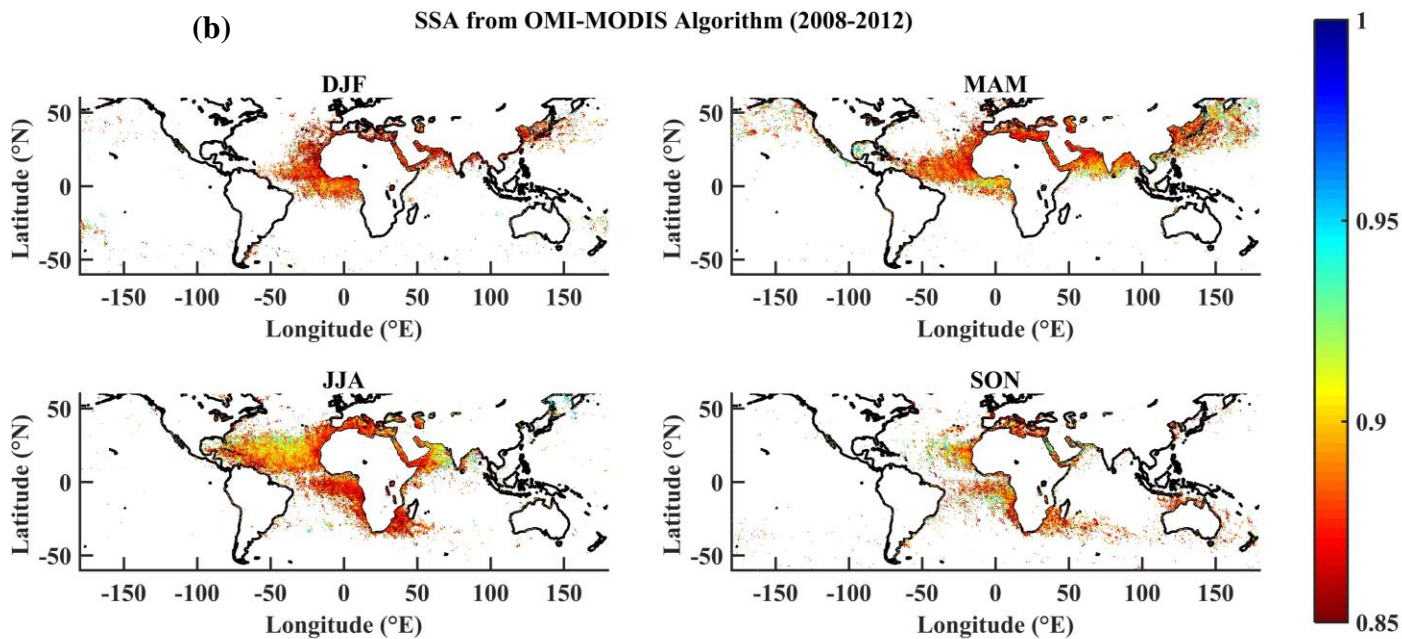
784 Wells, K.C., Martins, J.V., Remer, L.A., Kreidenweis, S.M., and Stephens, G.L.: Critical
785 reflectance derived from MODIS: Application for the retrieval of aerosol absorption over
786 desert regions, *J. Geophys. Res.*, 117(D3), doi:10.1029/2011JD016891, 2012.

787 Zhu, L., Martins, J.V., and Remer, L.A.: Biomass burning aerosol absorption measurements with
788 MODIS using the critical reflectance method, *J. Geophys. Res.*, 116(D7),
789 doi:10.1029/2010JD015187, 2011.

790 Zuluaga, M.D., Webster, P.J., and Hoyos, C.D.: Variability of aerosols in the tropical Atlantic
791 Ocean relative to African Easterly Waves and their relationship with atmospheric and
792 oceanic environments, *J. Geophys. Res.*, 117(D16), doi:10.1029/2011JD017181, 2012.

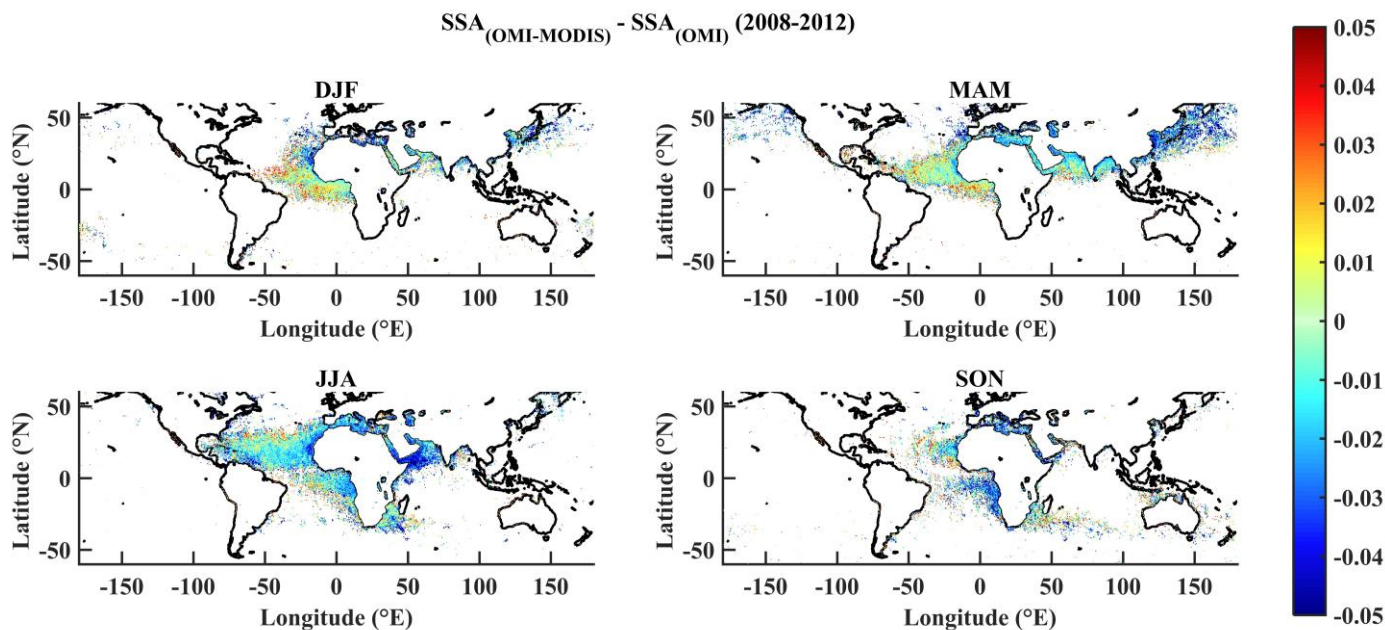


793



794

795 **Figure 1.** Spatial distribution of SSA at 388nm retrieved by a) OMI and b) OMI-MODIS. In the
 796 present study, points which had the same SSA value at the 5 discrete heights provided by OMI or
 797 an invalid value at any one height were considered invalid for the OMI-MODIS retrieval since
 798 interpolation was not possible. This resulted in the reduction of the number of valid points for
 799 OMI-MODIS when compared to OMI.

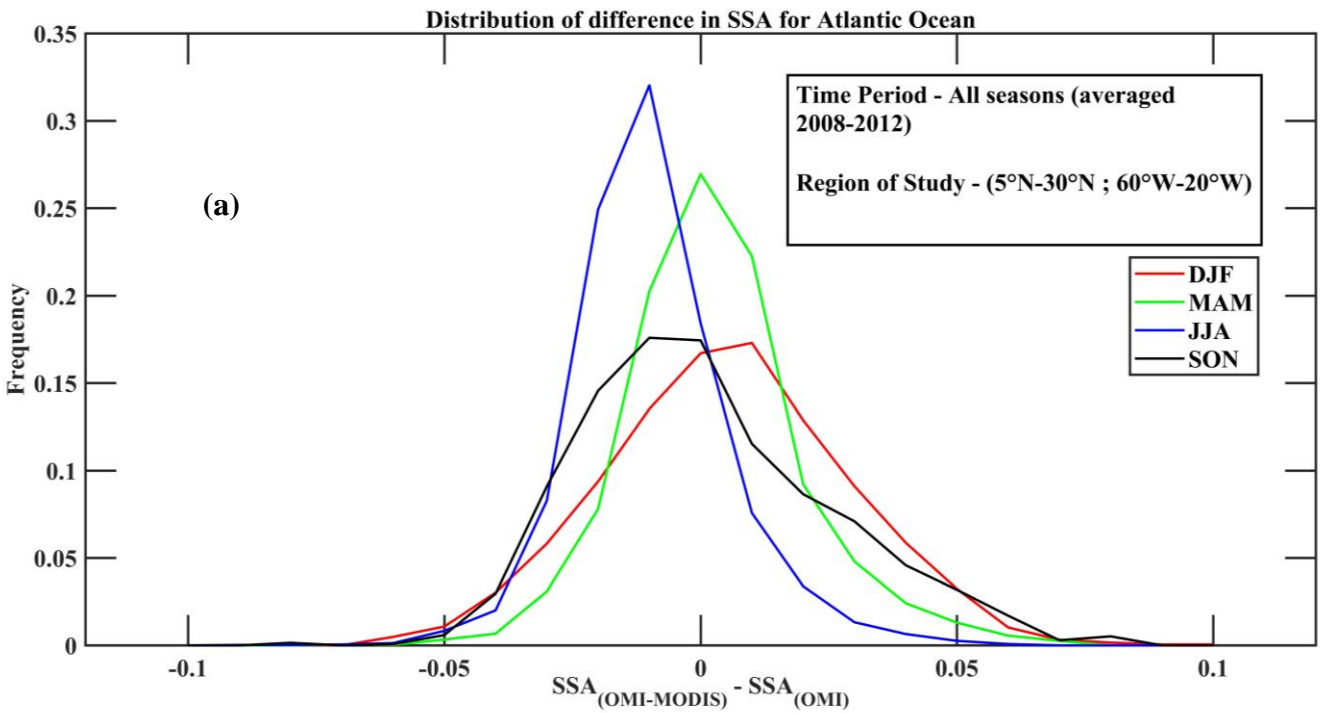


800

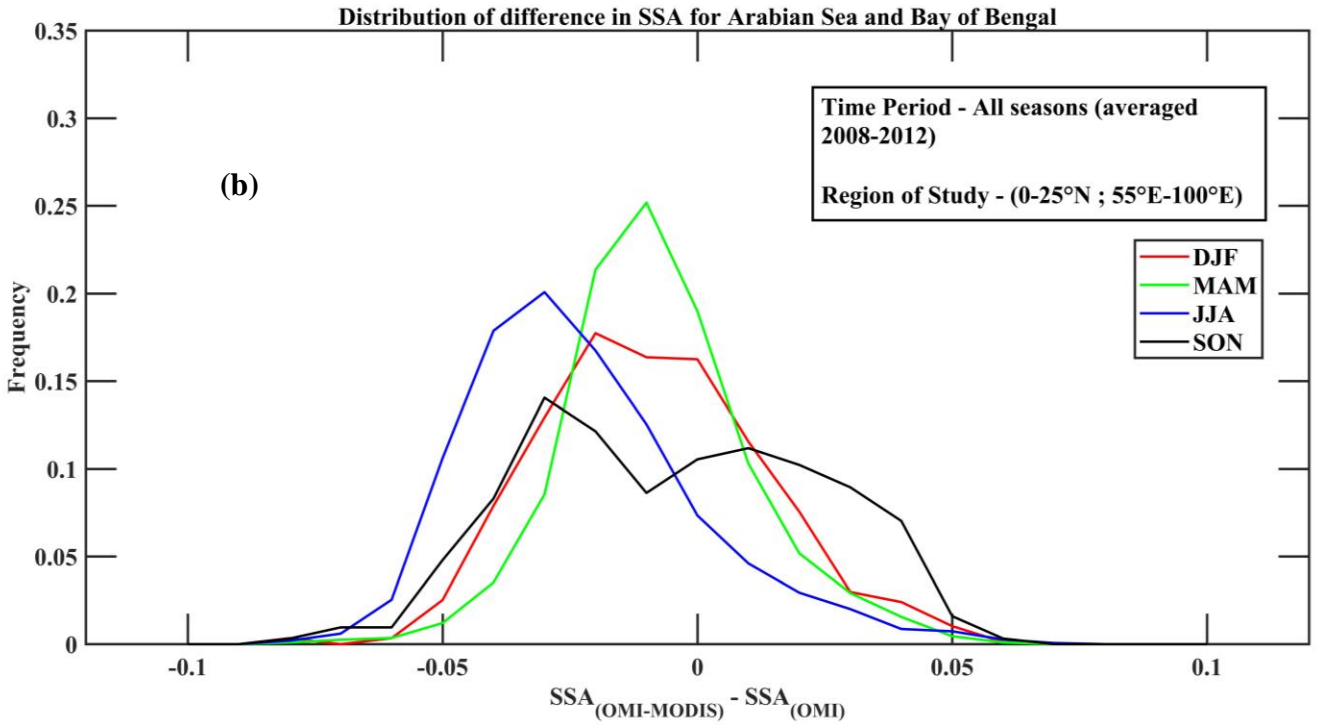
801 **Figure 2.** Spatial distribution of difference in SSA retrieved by OMI-MODIS and SSA retrieved
802 by OMI, both at 388nm. When the OMI-MODIS SSA value was found invalid, the difference
803 was also considered to be invalid.

804

805



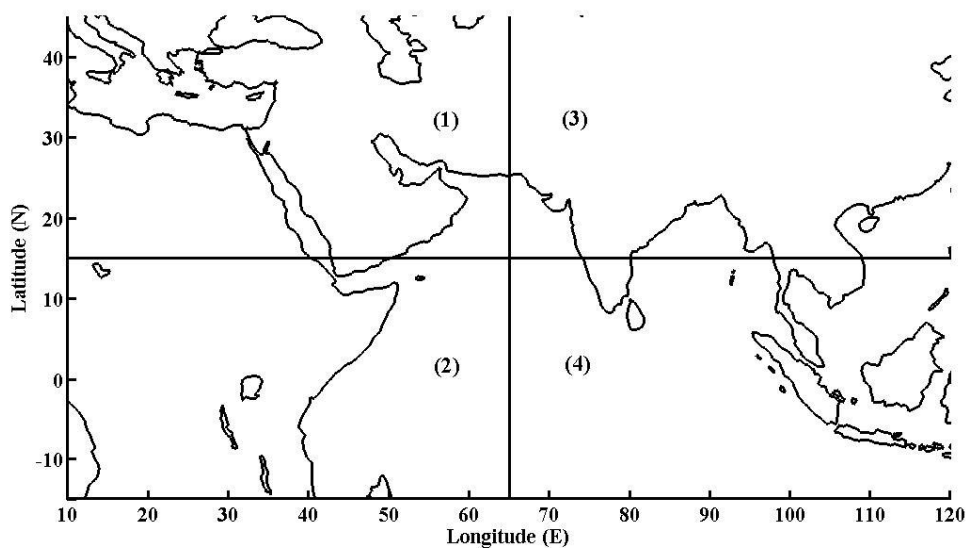
806



807

808 **Figure 3.** Distribution of difference in SSA for all seasons averaged over 2008-2012 over a)
 809 Atlantic and b) Arabian Sea and Bay of Bengal. It can be seen that over the Atlantic Ocean, 80%
 810 of the difference in SSA retrievals was within the ± 0.03 range. Over the Arabian Sea and Bay of
 811 Bengal, the retrievals agreed well during the MAM season when the region was influenced by
 812 dust.

813

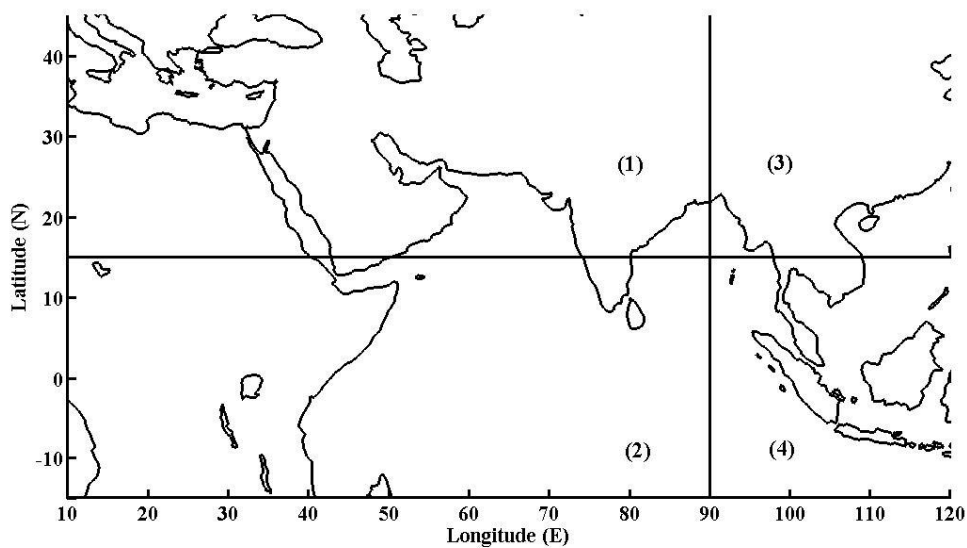


814

815 **Figure 4.** Regions representing the various aerosol sources for a point over the Arabian Sea. 1)

816 Arabian Peninsula and North Africa, 2) Central Africa, 3) Indian sub-continent and 4) Indian

817 Ocean and Southeast Asia.



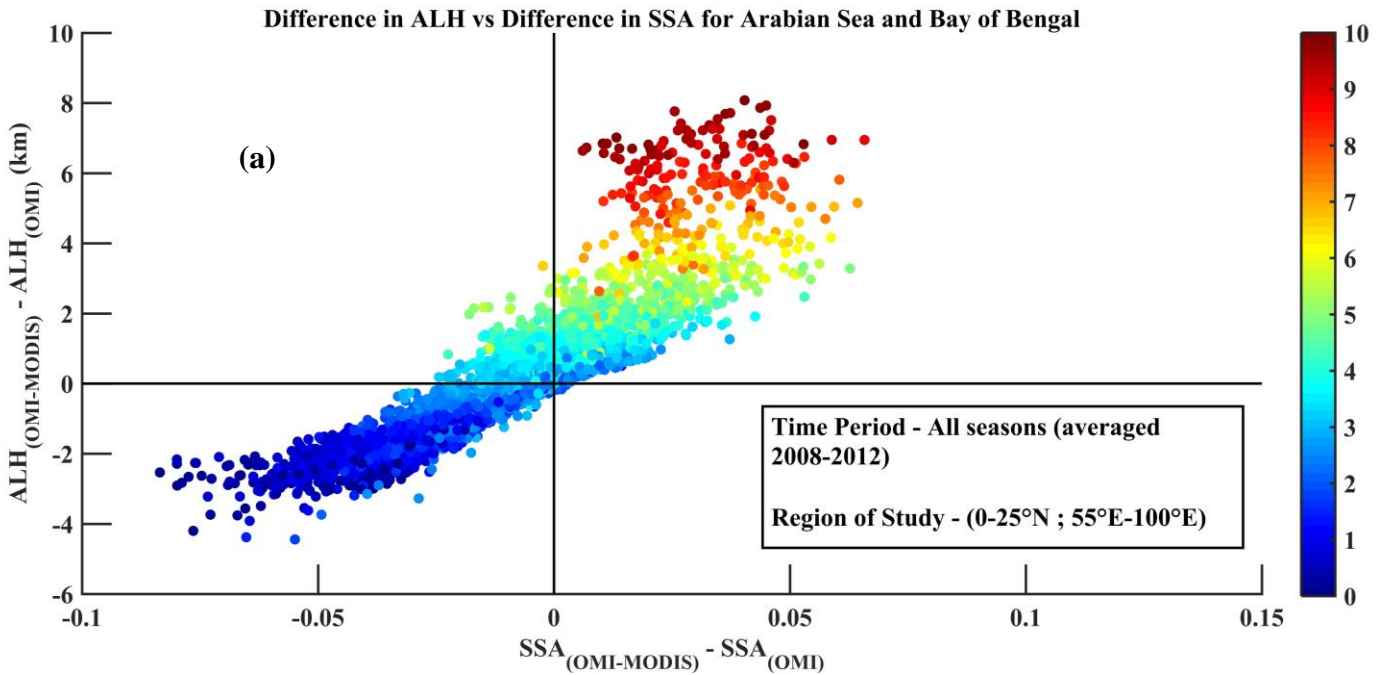
818

819 **Figure 5.** Regions representing the various aerosol sources for a point over the Bay of Bengal. 1)

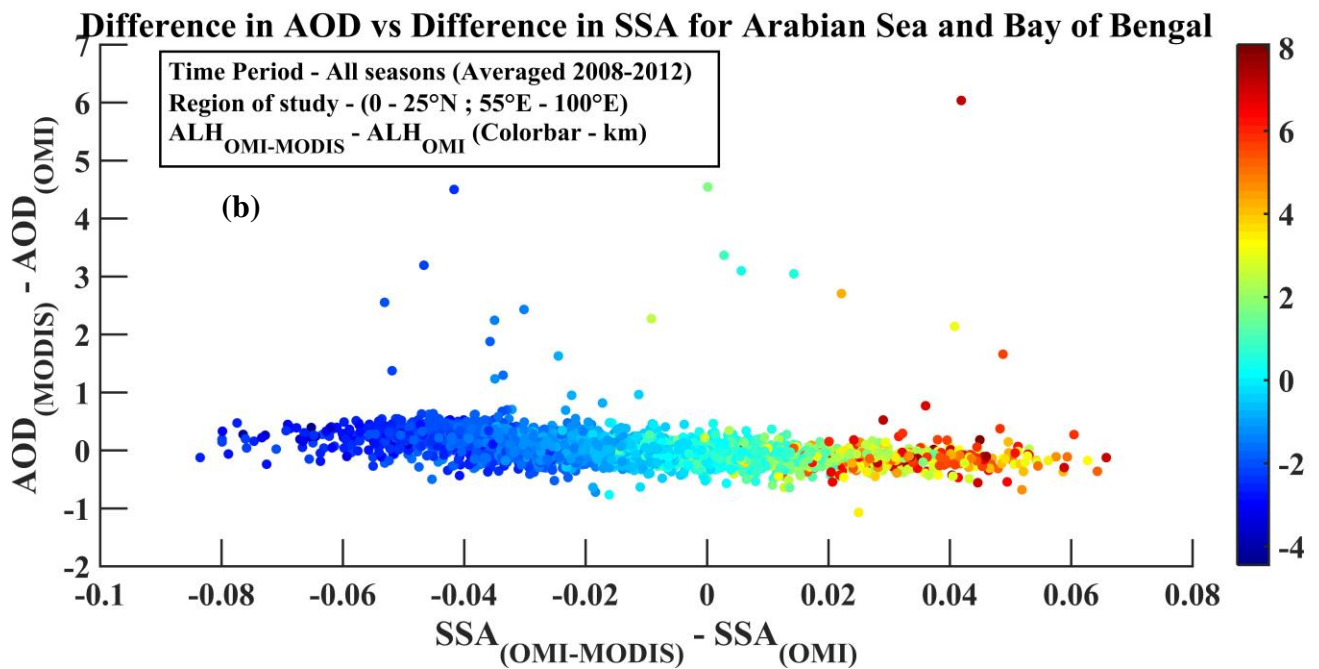
820 India/Arabian Peninsula, 2) Indian Ocean, 3) North/Northeast India and East Asia and 4)

821 Southeast Asia.

822



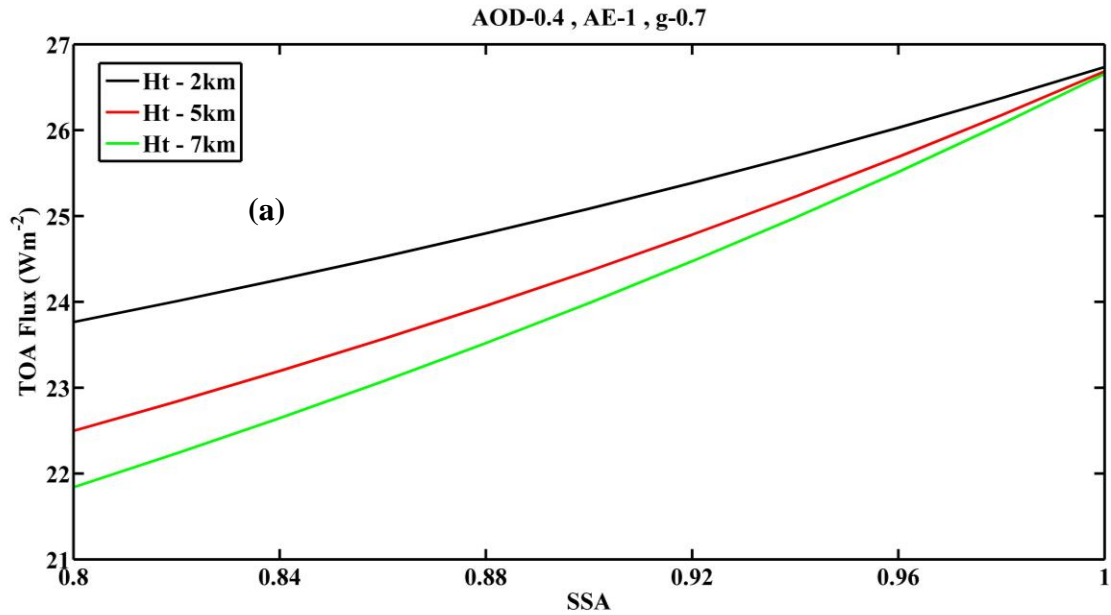
823



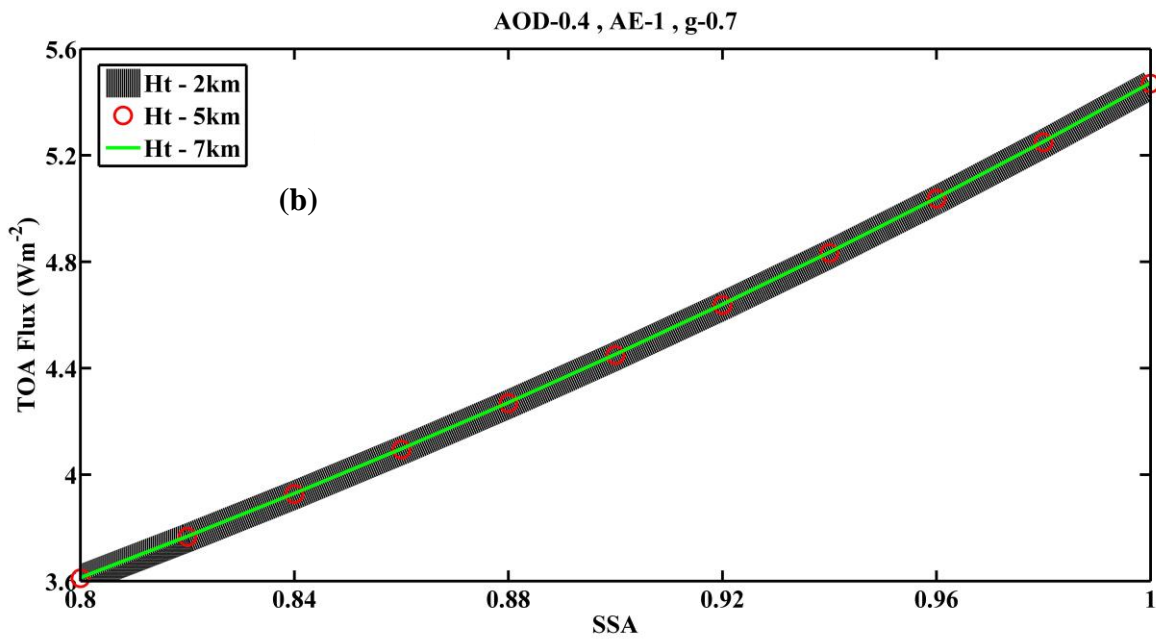
824

825 **Figure 6.** a) Difference in aerosol layer height (ALH - km) between OMI-MODIS and OMI vs.
826 difference in SSA over Arabian Sea and Bay of Bengal. The colorbar represents ALH estimated
827 by OMI-MODIS algorithm (km). At lower height (dark blue circles) estimated by OMI-MODIS

828 OMI overestimated SSA when the ALH was overestimated and vice versa at higher heights
 829 estimated by OMI-MODIS b) Difference in AOD ($AOD_{MODIS} - AOD_{OMI}$) has been plotted with
 830 difference in SSA ($SSA_{OMI-MODIS} - SSA_{OMI}$). An inverse relationship was observed. The colorbar
 831 represents the difference in aerosol layer height (ALH - km) between OMI-MODIS and OMI.
 832

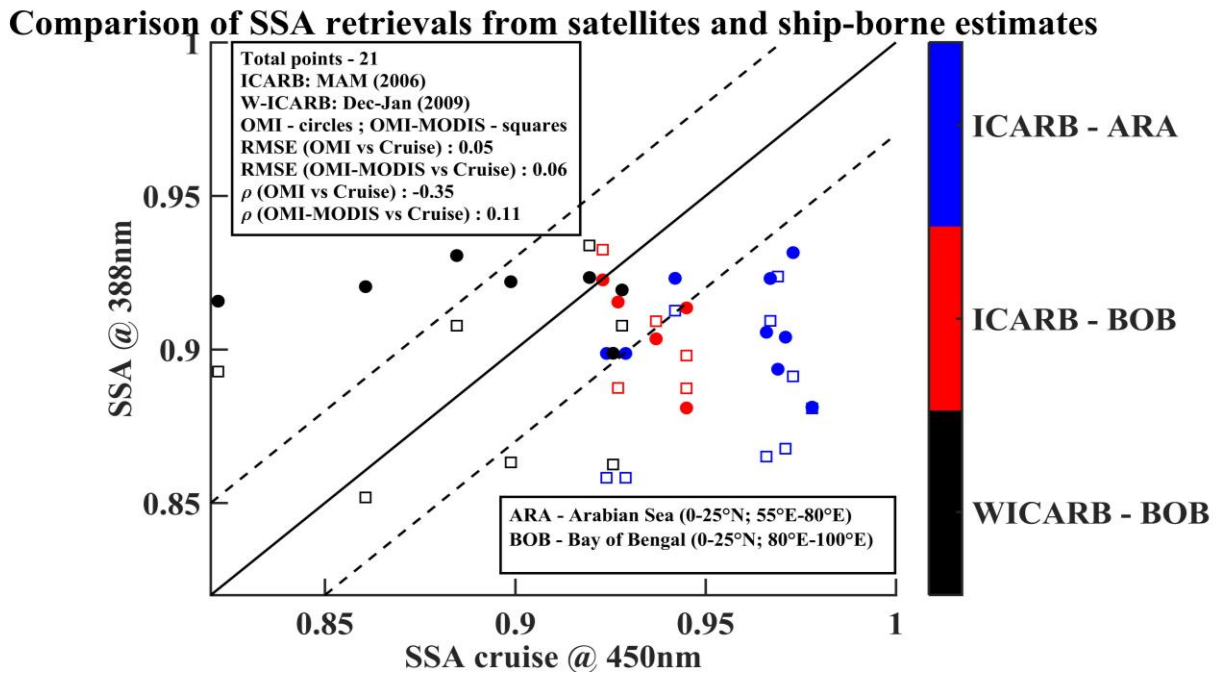


833



834

835 **Figure 7.** TOA flux calculated from SBDART for different SSA and ALH a) with Rayleigh
 836 scattering and b) without Rayleigh scattering for UV (300-400nm)



837
 838 **Figure 8.** Comparison of SSA_{OMI} (circles), $SSA_{OMI-MODIS}$ (squares) with cruise measurements.
 839 Each point represents the mean SSA in a 2° box surrounding each cruise location averaged over
 840 the respective cruise time period. Due to the sparse nature of OMI-MODIS retrieval, the total
 841 number of points common to both the cruise and satellite estimates is only 21. The solid black
 842 line is the $y=x$ line. The dotted lines represent ± 0.03 range. The colorbar represents the cruise
 843 name and the region where the measurements are taken. ICARB (Integrated Campaign for
 844 Aerosols, Gases and Radiation Budget) during March-April-May (MAM) 2006 season; W-
 845 ICARB (Winter ICARB) during December-January (2008-2009); ARA (Arabian Sea); BOB
 846 (Bay of Bengal). Discrepancies between the satellite retrievals and cruise measurements were
 847 seen during the ICARB cruise when elevated aerosols were predominantly present over both the
 848 regions which might not be detected by the cruise measurements.

References	Method	Technique	Limitation
Herman et al., 1975; King, 1979; Eck et al., 1998; Dubovik and King, 2000; Torres et al., 2005	Ground-based observations	Inverse methods measurements of solar radiances and/or aerosol properties along with radiative transfer calculations	Measurements are spatially and temporally constrained
Dubovik et al., 2002	Global network – Aerosols Robotic Network (AERONET)	Inverse technique using near-real time measured direct and diffuse radiation	Only land-based, low coverage over remote oceanic regions
Kaufman, 1987; Zhu et al., 2011; Wells et al., 2012	Critical surface reflectance - where the net role of aerosol absorption and scattering becomes independent of aerosol optical thickness and is affected only by SSA	Over varying surface reflectance, the radiance difference between clear and hazy skies is measured using satellite images	Limited spatial variability of surface reflectance. Works only for few cases where there are large amount absorbing aerosols present

Kaufman et al., 2002b	Retrieve SSA in visible wavelengths	Sun-glint is used as a bright background to differentiate role of scattering from aerosol absorption	Only limited scenarios present and does not work on land when absorbing aerosols are present (Torres et al., 2005).
Diner et al., 1998; Remer et al., 2005	Multi Angle Imaging Spectroradiometer (MISR) and Moderate Resolution Imaging Spectroradiometer (MODIS)	Retrieves AOD and SSA in the visible and infrared region of solar spectrum	Surface reflectance influences the retrievals
Herman et al., 1997; Torres et al., 1998	Total Ozone Mapping Spectrometer (TOMS)	Aerosol index parameter is highly sensitive to the Rayleigh scattering thus acting as a bright background in the UV regime	Large pixel size prone to cloud contamination
Torres et al., 2002	Ozone Monitoring Instrument (OMI)	Similar technique as TOMS. Pre-defined aerosol models used.	Sensitive to aerosol layer height and still prone to cloud contamination

849

850 **Table 1.** Ground-based and Satellite-based indirect methods to retrieve SSA

851

852

Seasons \ Regions		1	2	3	4
DJF	500m	57%	0%	38%	5%
	1500m	62%	10%	19%	9%
	2500m	81%	14%	0%	5%
MAM	500m	19%	43%	19%	19%
	1500m	29%	29%	23%	19%
	2500m	57%	14%	24%	5%
JJA	500m	0%	24%	0%	76%
	1500m	19%	67%	0%	14%
	2500m	62%	33%	5%	0%
SON	500m	5%	24%	47%	24%
	1500m	14%	19%	48%	19%
	2500m	38%	10%	19%	33%

853

854 **Table 2.** Influence of various aerosol sources over Arabian Sea given as percentage of

855 trajectories originating from each source respectively. The maximum influence is given in black

856 bold. The different source regions are explained in text and Fig. 4.

Seasons \ Regions		1	2	3	4
		DJF	500m	72%	0%
1500m	48%		14%	10%	28%
2500m	29%		33%	0%	38%
MAM	500m	19%	48%	0%	33%
	1500m	57%	29%	20%	14%
	2500m	71%	24%	0%	5%
JJA	500m	0%	100%	0%	0%
	1500m	5%	95%	0%	0%
	2500m	14%	81%	0%	5%
SON	500m	5%	52%	33%	10%
	1500m	5%	43%	43%	9%
	2500m	5%	33%	29%	33%

858

859 **Table 3.** Influence of various aerosol sources over Bay of Bengal given as percentage of
860 trajectories originating from each source respectively. The maximum influence is given in black
861 bold. The different source regions are explained in text and Fig. 5.

862